論文 / 著書情報
Article / Book Information

題目(和文)	
Title(English)	Development of Versatile Channel Sounder for Multi-link MIMO Channel Characterization at 11 GHz
著者(和文)	小西洋平
Author(English)	Yohei Konishi
出典(和文)	学位:博士（工学）, 学位授与機関:東京工業大学, 報告番号:甲第9795号, 授与年月日:2015年3月26日, 学位の種別:課程博士, 審査員:高田　潤一,山下　幸彦,鈴木　博,荒木　純道,府川　和彦
Citation(English)	Degree:, Conferring organization: Tokyo Institute of Technology, Report number:甲第9795号, Conferred date:2015/3/26, Degree Type:Course doctor, Examiner:,,,,
学位種別(和文)	博士論文
Type(English)	Doctoral Thesis

Doctoral Dissertation

Development of Versatile Channel Sounder for Multi-link MIMO Channel Characterization at 11 GHz

Yohei Konishi

Professor Jun-ichi Takada
Adviser

Department of International Development Engineering
Tokyo Institute of Technology

Acknowledgment

The Ministry of Internal Affairs and Communications of Japan is acknowledged for supporting this research under the governmental project of "The research and development project for expansion of radio spectrum resources".

Foremost, I would like to express my sincere gratitude to Prof. Jun-ichi Takada, my doctoral adviser, who allowed me to study in his laboratory and continuously encouraged me by providing appropriate suggestions. I was strongly inspired by his immense knowledge, passion for engineering research and compassion for students.

I kindly appreciate my doctoral examination committee: Prof. Hiroshi Suzuki, Prof. Kiyomichi Araki, Assoc. Prof. Kazuhiko Fukawa, Assoc. Prof. Yukihiko Yamashita, and Assoc. Prof. Kei Sakaguchi.

My thanks also goes to Asst. Prof. Minseok Kim, who directly instructed me all the time during the channel sounder development. It was not only the academic knowledge but also I learned a lot from his attitude on research.

To people from Suzuki-Fukawa laboratory, Asst. Prof. Satoshi Suyama, Mr. Shunsuke Kato and Mr. Hiroyuki Fukuda: without their generous support through the calibration of transmission hardware, it would have been impossible to realize the channel sounder.

To many members who worked together in the MIC project, Dr. Yuyuan Chang, Ms. Yiang Miao, Mr. Boxing Gao, Mr. Yuta Maruichi, Mr. Pham Hue Van, Mr. Pham Kinh Vun and Mr. Shizhi Zhang: I certainly believe that the channel sounder would not be realized without your substantial

contributions.

To people from Takada laboratory, I was very happy to share time with you in laboratory. I hope we could see in the future at somewhere in the world, as the family of Takada laboratory.

My special gratitude goes to Prof. Toyohiko Ishihara, Dr. Keiji Goto and Dr.Tohru Kawano of National Defense Academy. Their ideas and attitudes on the study of electromagnetic wave propagation lead me the field of research. I also wish to thank people of Japan Grand Self-Defense force, Ministry of Defense, Japan, for giving me this precious opportunity to study at Tokyo Institute of Technology.

Last but not the least, I would like to thank my loving family Chie, Yukiko and Kakeru. Your dedicated supports and smiles were the true driving force of my study.

Abstract

The recent explosion of mobile Internet usage results in the need for higher data rates in mobile applications. If this trend continued, it has projected in [1] that data rates of several tens of Gbps will be required in the future mobile systems. To achieve such a high data rates, use of multiple-input-multiple-output (MIMO) technology with bandwidth of several hundreds of MHz will be mandatory requirements. However due to the congestion of conventional frequency spectrum used for mobile systems, it will be unavoidable to shifts the operating spectrum towards unoccupied higher microwave bands.

On the other hand, achievable MIMO multiplexing gain in the real environment at higher frequency have not yet been fully revealed. Increase in propagation and shadowing loss at higher frequency limits the communication coverage, so it may limits the available parallel propagation channels due to the existence of significant line-of-sight (LoS) components. Moreover the channel property will be more specific to individual environment. Therefore, it should be necessary to characterize the channel properties in the field measurement. In particular, the analysis and design of multi-link scenarios such as mult-iuser MIMO and base station cooperation will be important to compensate the reduction in MIMO independent paths. This requires more sophisticated channel models of correlation among links and the ranks of the channels.

The inherent motivation of this work is to implement wideband channel sounding functionality to generic MIMO system testbed. This strategy en-

ables simultaneous testing of transmission performance and MIMO channel properties. In this regard, 24×24 MIMO channel sounder at 11 GHz is developed based on a scalable fully-parallel MIMO architecture so that it can be flexibly configured with 3 transmitter and 3 receiver casings. This flexibility allows the measurement for various purposes including double-directional channel modeling and investigation of multi-link MIMO communication systems. Implementation issues related to the multi-link operation and the fully-parallel architecture are successfully solved by appropriate system design and applying several calibration techniques. Performance of the developed system is validated by various evaluation experiments. Finally, multi-link channel characteristics in an indoor environment are investigated utilizing the system developed in this study. The results demonstrate the capability of the system for channel modeling in future mobile communication systems.

Contents

List of Figures

List of Tables

Chapter 1

Introduction

1.1 Overview

The rapid growth of mobile Internet usage results in the demand for further increase in data rate and system capacity. Although the use of multiple-input-multiple-output (MIMO) transmission [2, 3, 4] is a promising solution to improve spectral efficiency, its benefits rely on the uncorrelated fading between antenna elements which will not always be satisfied in the practical systems (array is packed in a compact terminal) and environments (ill-conditioned propagation channel). Moreover due to the congestion in frequency spectrum under 5 GHz, spectrum shift toward higher frequency bands will be one of the most possible solutions to satisfy the traffic demands required [5]. At frequency bands above 6 GHz, increase in path loss and shadowing loss will limit the cellular coverage, and radio channels received at multiple antennas will be more correlated as illustrated in Figure 1.1. In addition, influence of Doppler frequency shift in a dynamic radio environment will also increase with the carrier frequency.

For these reasons, multi-link cooperative transmission technology is attracting a lot of attention as a key enabler for high data-rate and high capacity wireless systems in the fourth-generation (4G) [6] and beyond. Basically, the concept of multi-link technology includes joint signal processing among

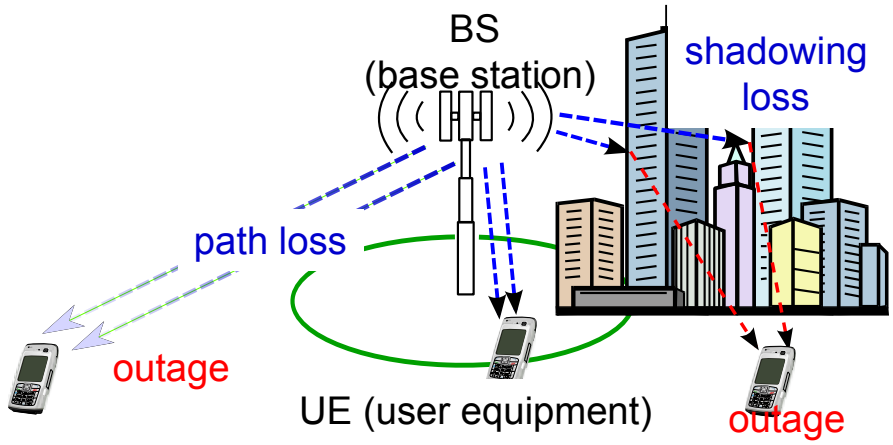

Figure 1.1 Illustration of propagation channel properties when higher frequency is utilized.

spatially distributed multiple user equipments (UEs) and/or base stations (BSs), which provides more spatial diversity gain compared with conventional single-link MIMO systems. Multi-user MIMO (MU-MIMO) [7] and coordinated multi-point (CoMP) [8] networks which utilize the spatial diversity among UEs and BSs, respectively, have recently attracted much interest not only to satisfy the requirements in 4G but also for further performance enhancement [9].

However, the performance of multi-link MIMO systems will be heavily dependent on the level of channel correlation between different links [10, 11]. Moreover since each of the UEs and BSs will also be equipped with multiple antennas, directional characterization both at transmitter (Tx) and receiver (Rx) is also important for the design of antenna arrays. Accordingly, there must be a strong demand for a flexible and versatile measurement system suitable for the purposes mentioned above. It should offer a more detailed channel analysis from two important aspects of the evaluation of MIMO transmissions system and the investigation of physical radio propagation mechanisms.

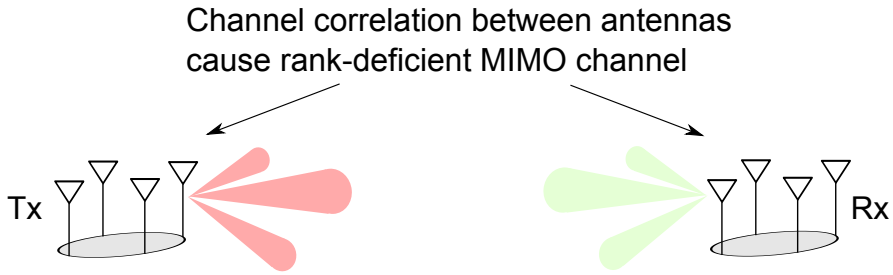

Figure 1.2 Conventional single-link MIMO systems that utilize multi-antenna adversity. Appropriate antenna design is necessary to avoid signal correlations between antenna elements.

1.2 Benefits of Multi-link MIMO Systems

Considering a MIMO system with N_{tx} antennas at the Tx, and N_{rx} antennas at the Rx, the time-variant channel transfer function between the jth Tx antenna and the ith Rx antenna is denoted by $H_{i,j}(t, f)$, where t is the observation time and f is the frequency. The MIMO channel matrix can be written by

$$\mathbf{H}(t,f) = \begin{pmatrix} H_{11}(t,f) & H_{12}(t,f) & \cdots & H_{1N_{\text{tx}}}(t,f) \\ H_{21}(t,f) & H_{22}(t,f) & \cdots & H_{2N_{\text{tx}}}(t,f) \\ \cdots & \cdots & \ddots & \vdots \\ H_{N_{\text{rx}}1}(t,f) & H_{N_{\text{rx}}2}(t,f) & \cdots & H_{N_{\text{rx}}N_{\text{tx}}}(t,f) \end{pmatrix}. \tag{1.1}$$

Theoretical channel capacity in fading channel derived in [4] is maximized if all the elements of H_{ij} are distributed as circular-symmetric complex-Gaussian independent identically (i.i.d.). In this ideal channel condition, the MIMO channel matrix becomes full-rank, hence simultaneously transmitted multiple signal streams can be separated at receiver side (spatial multiplex-

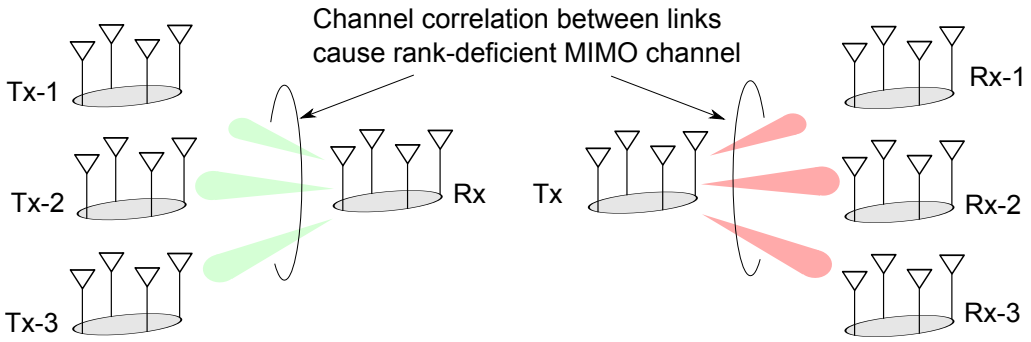

Figure 1.3 Multi-link MIMO systems that utilize spatial diversity among spatially distributed transmitters and receivers.

ing). However, i.i.d. fading channel can not be always realized in practical systems and environment where antenna elements can not be spaced so large, especially at user equipments (Figure 1.2). Moreover, channel itself will be rank-deficient when higher frequency is used since Tx and Rx link have to has line-of-sight (LoS) like condition keeping required signal-to-noise-power-ratio (SNR) to cover increased propagation loss.

In this regard, multi-link MIMO systems that exploit spatial diversity among multiple UEs and/or BSs is attractive for the improvement of total system capacity. The benefits of multi-link MIMO systems come from the reduced channel correlation among UEs and/or BSs thanks to scattered UEs/BSs distribution.

It is obvious that multi-link MIMO gain over the single-link MIMO system is still dependent on the level of inter-link correlation as shown in Figure 1.3, where most of the existing studies assumed sufficiently low correlation between links. Although there exist several measurement-based evaluation to confirm the benefit of multi-link MIMO system, channel models obtained from channel sounding campaign are very limited [12, 13, 14] due to the lack of multi-link MIMO channel sounder. In [14], multi-link correlation phenomena in an indoor environment was investigated by using dual-link MIMO

channel sounder [15]. The significance of common scatterers at two links was identified as the cause of inter-link correlation. This concept should be confirmed in various channel environments and system configurations.

1.3 Prior Studies

To date, a lot of measurement systems for the evaluation of MIMO wireless applications have been developed. Basically, the hardware architecture determines the fundamental capability of channel sounder. The most commonly used architecture is the switched array system which consists of single Tx and single Rx RF ports, and they are shared among the array antennas with RF multiplexer (e.g. [16]). Although switching sounder significantly reduces cost and complexity, the number of antennas to be switched usually limits the channel acquisition rates, thus the measurement in some environments with high Doppler frequency is difficult to be managed. The trade-off between the measurement speed (MIMO snapshot rate) and hardware complexity in various channel sounder architecture is shown in Figure 1.4. The drawback can be avoided by using parallel architecture at receiver side. Obviously, N_{rx} channels at the receiver can be simultaneously measured, so the measurement time can be reduced by $1/N_{\mathrm{rx}}$ of switching sounder. The MIMO snapshot rate must be first enough since it determines the measurable Doppler frequency due to the time-variant radio channel. Moreover as shown in Figure 1.5, the influence of Doppler shift will be increased according to the center frequency. It should be noted that simultaneous transmission can not reduce the measurement time to keep the orthogonality of transmission signals. Therefore, the use of fully-parallel MIMO architecture is considered as the optimal architecture when only the single-link measurement is targeted. However, the same hardware can be utilized in fully-parallel channel sounder for both transmission evaluation and channel sounding simultaneously.

Existing channel measurement systems can be classified into two categories as follows based on the purpose of evaluation.

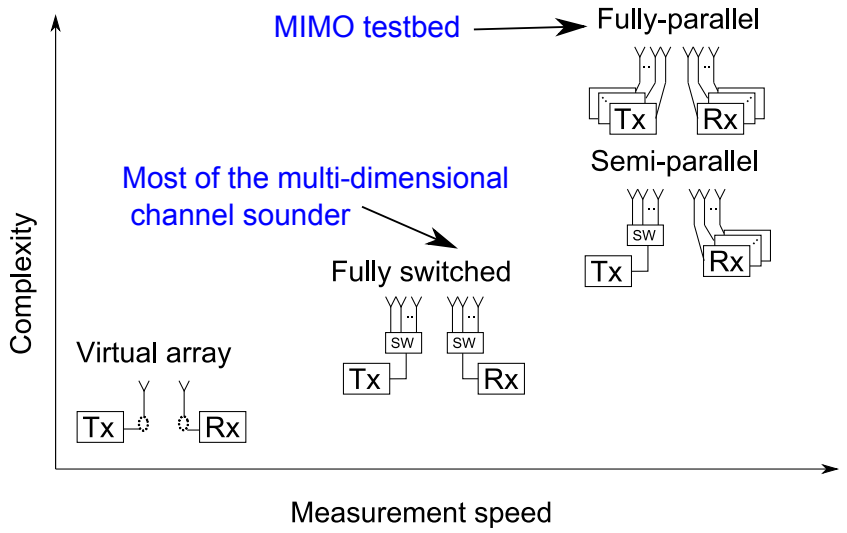

Figure 1.4 Comparison of sounder architecture in terms of MIMO snapshot rate and hardware complexity.

1. MIMO system testbeds
   MIMO testbeds focus on the performance evaluation of specific MIMO transmission systems. It basically requires real-time processing based on fully-parallel MIMO architecture for the practical evaluation of transmission performances. Although the same hardware can be utilized for the channel sounding purpose as in [17, 18, 19], directional channel estimation has never been considered in fully-parallel architecture due to its hardware complexity. Moreover, there exist several practical issues to fictionalize generic MIMO testbed into channel sounder, such as synchronization between transmitter (Tx) and receiver (Rx) and back-to-back calibration to remove the influence of hardware from measured channel transfer characteristics.

2. Multi-dimensional MIMO channel sounders
   Multi-dimensional channel sounders [20] focus on the investigation of physical radio propagation mechanisms. Fully-switched array architec-

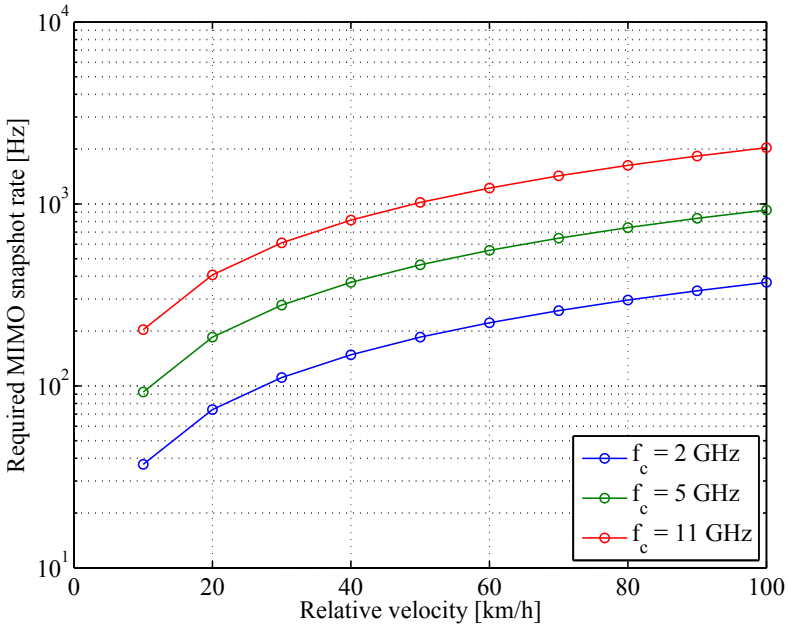

Figure 1.5 Requirement of MIMO snapshot rate to measure Doppler effect.

ture that has a single radio front-end at both sides of Tx and Rx has been widely employed (e.g. [16, 21, 22, 23]) due to its cost-effectiveness, simple hardware implementation and easy calibration [24]. Such systems realize the double-directional analysis of propagation channel [25], but are mainly designed for the point-to-point MIMO channel characterization due to the difficulty in synchronization among multiple links. Also in the fully-switching architecture, temporal channel acquisition rate is usually limited by the time for array switching, hence the measurable maximum Doppler frequency will be restricted.

3. Measurement Systems for Multi-link Wireless Applications
   Figure 1.6 shows the currently proposed multi-link channel measurement techniques.

   (a) Single sounder sequential measurement

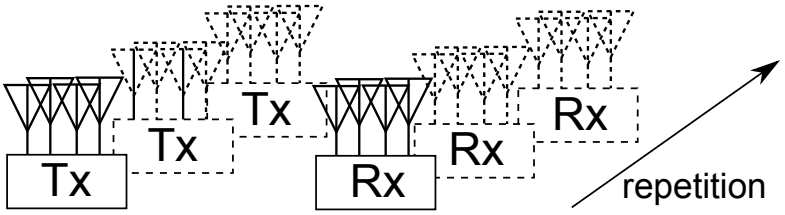

(a) Sequential multi-link measurement. Use single channel sounder and repeat the measurement by moving equipments. The selected measurement points are treated as multiple Txs or Rxs.

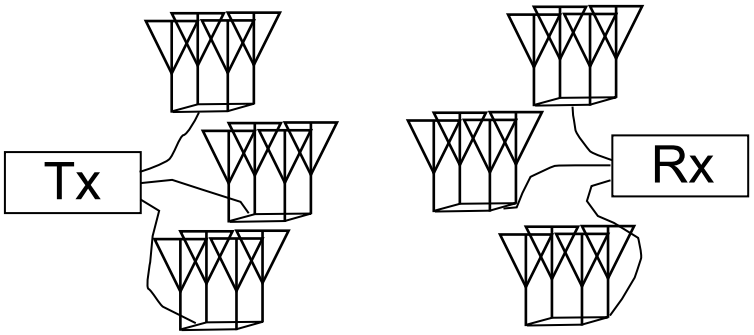

(b) Distributed antenna technique. Use single channel sounder but distribute antenna array via long RF cables.

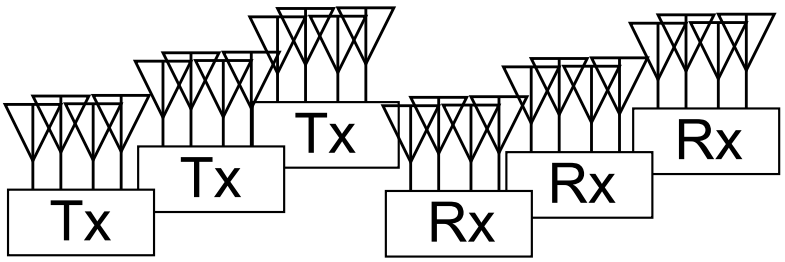

(c) Real-time multi-link measurement. Multiple channel sounders are required.

Figure 1.6 Schematics of several multi-link measurement techniques.

(b) Distributed antenna measurement

(c) Synchronized simultaneous measurement using multiple channel sounders

Testbeds for multi-link MIMO networks have also been developed to evaluate multi-link cooperation gain in practical environments e.g. [26, 27, 28, 29, 30]. The required level of synchronization (time, frequency and phase) basically depends on the selected cooperation scheme. For example, joint transmission and/or reception in CoMP networks require precise phase synchronization among BSs. It can be realized either by central processing unit with remote radio heads (RRHs) [26] or by sharing a common carrier among BSs via optical fibers. However, it significantly increases the development cost, and also limits the flexibility to evaluate various measurement environments. A channel sounder for the double-directional channel investigations of multiple links was reported in [15]. The system is composed of two individually developed fully-switching MIMO channel sounders (single Tx and two Rxs). Frequency synchronization is achieved by a highly stable atomic oscillator which is used as the reference for local oscillators (LO) at each of the distributed devices. Array switching sequences are not synchronized since two Rxs are individually designed. This timing offset at two Rxs can be estimated and removed in post-processing thanks to the same switching periods at Rxs (both of Rxs have same elements of array). Although its capability in estimating directional channel both at Tx and Rx with high resolution is valuable, the single Tx dual-link scenario will not be enough to cover a large variety of multi-link scenarios including MU-MIMO (i.e. distributed UEs) and CoMP (distributed BSs) networks. Several multi-link channel measurement techniques have also been proposed as summarized in [11] for some limited measurement scenarios. In [31] and [32], multi-link channel measurements were realized based on a single sounder distributed antenna technique. In this method, frequency and phase synchronization can be achieved by connecting multiple antenna arrays to single MIMO sounder via RF cables.

However, the measurement range is restricted by the loss in RF cables, so the applicable measurement scenarios are limited.

In summary of prior studies, specifications of existing channel sounders used in multi-link measurements are summarized in Table 1.1. It is clear that although there exist many measurement systems focusing on transmission performance evaluation of MIMO systems or investigation of MIMO propagation mechanisms, no system can be found covering both the aspects of transmission evaluation and physical radio channel. Only the multi-link channel sounder capable of investigating physical radio propagation mechanism developed by the collaboration ob Lund and Aalt universities [15], system flexibility is very limited so the evaluation of various multi-link MIMO applications to be considered in future wireless communication systems is still difficult.

It should be also noted that all of the prior studies focused on the frequency bands between 2 - 5 GHz, and usability of MIMO applications at unused higher microwave band above 6 GHz is not sufficiently investigated, where both of the transmission performance and influencing propagation properties will be different from lower frequency bands.

1.4 Motivations for Study

As described in Section 1.1, there is a strong demand on the significant system capacity improvement in 4G and beyond. There are several novel transmission technologies such as conventional MIMO and multi-link MIMO, and utilization of higher frequency spectrum. However, since the benefits of MIMO transmission result from spatial diversity which depends on the characteristics of physical propagation channel and operating frequency band, radio channel have to be sufficiently investigated for the proper system design and development. Therefore, one of the strong motivation of this thesis is to contribute the realization of 4G and beyond from the view point of radio channel propagation.

Table 1.1 Specifications of Existing Sounders used in Multi-link Measurements.

Parameter	LU-Aalt (RUSK) [15]	Eurocom EMOS [33]	RUSK-Stanford [34]
Center frequency	5.3 GHz	800 MHz, 1.9 GHz	2.45 GHz
Bandwidth	120 MHz	4.8 MHz	240 MHz
Transmit power	30 dBm	30 dBm	N/A
Architecture	switching	parallel	switching
Num. of Tx antenna	30	4	8
Num. of Rx antenna	30	2	8
MIMO snapshot rate	25.4 Hz	375 Hz	N/A
Synchronization	Rubidium	over-the-air	Rubidium
Multi-link mea. method	real-time	real-time	distributed ant.

cont'd

RUSK-Ilmenau [35]	EASY-C (Berlin) [36]	EASY-C (Dresden) [36]	**Titech. (this thesis)**
2.53 GHz	2.53 GHz	2.53 GHz	11 GHz
80 MHz	20 MHz	21.25 MHz	400 MHz
46 dBm	41 dBm	41 dBm	23.8 dBm
switching	parallel	parallel	parallel
16	16	2	24 (8)
48	10	16	24 (8)
75 Hz	500 Hz	1150 Hz	3400 Hz
Rubidium	optical fiber	GPS	Cesium
sequential	real-time	real-time	sequential (real-time)

From the view point of engineering research, role of measurement-based radio channel characterization for several research fields such as service operation, transmission scheme and antenna, have to be clearly determined in the design of MIMO channel sounder. Basically, the service operators are interested in site-specific channel properties, while stochastic channel models generalized as mathematical form derived at a cost of reality are required for the development of transmission scheme. However when higher frequency is used where channel properties will be much different in individual environments (i.e. it may be difficult to develop channel model for canonical environments such as urban, rural etc.), the importance of measurement-based channel characterization is solid in every aspects of system developments including hardware implementation. Contributions to every aspects of transmission performance evaluation, antenna design and hardware imple-

mentation is also the motivation of this thesis.

1.5 Problem Statement

Based on the review of prior studies related to the evaluation of MIMO system performance and the investigation of propagation channel, novel architecture and channel sounder are identified as essential for the practical development of multi-link MIMO communication systems. Use of fully-parallel MIMO architecture in channel sounder that is advantageous in extensibility to the transmission evaluation is adopted in this thesis, but several practical issues have to be solved as follows.

- Synchronization method among spatially distributed devices
- Choice of frequency reference source for channel sounding purpose and its actual performance
- Design of hardware performance to be used and its actual performance
- Compensation method for hardware imperfections and its simple implementation for field measurement
- Development of back-to-back calibration technique for fully-parallel MIMO sounder

1.6 Objectives

The goal of this thesis is to develop channel sounder for multi-link MIMO channel characterization at 11 GHz with 400 MHz bandwidth. The system has to be flexible for the evaluation of various multi-link scenarios which is under consideration as candidate technologies in 4G and beyond. More specifically, the system should be capable of measuring both of the transmission performance and physical propagation mechanism, due to the expected

channel properties at 11 GHz which is sensitive to the individual environments. By applying the comparative analysis on the observed MIMO transmission performance and identified propagation mechanism, channel parameters and physical propagation phenomena critical to the multi-link MIMO transmission systems can be clarified.

The thesis particularly focuses on the implementation of hardware and verification of system performance that clarify the actual pros and cons of proposed fully-parallel MIMO channel sounder architecture. Besides the architectural discussions, achievable hardware performance at 11 GHz with 400 MHz bandwidth and its impact on channel sounder performance have to be evaluated. Since the developed channel sounder shares the hardware architecture with generic transmission system, this evaluation is directly comparable in the development of MIMO transmission systems at 11 GHz with 400 MHz bandwidth.

1.7 Limitations of this Thesis

Despite the sufficient channel sounder performance verified in this thesis, there exists several limitations that are remained as future considerations.

- Compensation of frequency dependent hardware imperfection
  In the implemented hardware compensation techniques for baseband circuits and RF analog-front-end, the imperfections are assumed to be frequency independent across system bandwidth of 400 MHz.

- Compensation of non-linear distortion in RF analog-front-end
  In the system performance evaluation, relatively significant 2nd harmonic was observed. The compensation of this non-linear distortion was not considered in this study since the level of the distortion was sufficiently small.

1.8 Related Works

It should be noted that the channel sounder described in this thesis was realized thanks to a lot of related works. Since it was impossible to include all the achievements from the related works, representative references are listed as follows.

- Scalable channel sounding scheme and system design [37]
  Scalable channel sounding technique for a fully parallel transceiver architecture that employs a layered scheme of frequency and space-time division multiplexing is based on this work. The influence of the transceiver imperfections on the measurement accuracy is also discussed based on the computer simulation which provided the desired compensation quality.

- Automatic IQ imbalance compensation technique for quadrature modulator [38]
  An automatic IQ imbalance compensation technique for quadrature modulators by using spectrum analyzer and feedback control is based on this work.

1.9 Overview of this Thesis

The rest of the dissertation is organized as follows.

Chapter 2: Measurement Systems for MIMO Applications
Implementation issues to realize multi-link fully-parallel MIMO channel sounder is presented based on the detailed review of existing measurement systems including MIMO system testbed, multi-dimensional MIMO channel sounder and multi-link MIMO evaluation systems. Design considerations for multi-link MIMO channel sounder to be developed are also discussed in terms of hardware architecture and synchronization method. By presenting the

proposed scalable fully-parallel MIMO sounder architecture and flexible synchronization method, pros and cons of the proposed system architecture is also discussed in this chapter.

Chapter 3: System Implementation
This chapter presents main contribution of this thesis, realization of channel sounder for multi-link MIMO channel characterization. Implemented channel sounding methodology, realized hardware components and calibration method are described together with the methodology for synchronized data acquisition among spatially distributed receivers.

Chapter 4: Performance Evaluation
Results of performance evaluation tests are presented. Influence of separated frequency references at Tx and Rx systems, phase noise stability and receiver sensitivity were evaluated. To verify the total system performance after applying several compensation techniques for hardware imperfection and back-to-back calibration, measurement results were compared with commercial vector network analyzer (VNA).

Chapter 5: Measurement Campaign
Results from indoor measurement campaign using the developed channel sounder are presented. The measurement aimed at testing the developed system in practical measurement environment, and demonstrating the system capability.

Chapter 6: Conclusion
The achievement and contributions of this work are summarized. Several considerations in the future research are also presented for the further utilization of the achievements in this thesis.

Chapter 2

Measurement Systems for MIMO Applications

2.1 Existing Measurement Systems

This section provides the detailed review of existing channel measurement systems. Based on the brief discussion in Chapter 1, MIMO system testbed and multi-dimensional MIMO channel sounder are first investigated. Then, existing multi-link measurement techniques are discussed for the appropriate system design in this thesis.

2.1.1 MIMO System Testbed

MIMO testbeds focus on the performance evaluation of specific MIMO transmission systems. It basically requires real-time processing based on fully-parallel MIMO architecture for the practical evaluation of transmission performances. Although the same hardware can be utilized for the channel sounding purpose as in [17, 18, 19], directional channel estimation has never been considered in fully-parallel architecture due to its hardware complexity.

Testbeds for multi-link MIMO networks have also been developed to evaluate multi-link cooperation gain in practical environments e.g. [26, 27, 28,

29, 30]. The required level of synchronization (time, frequency and phase) basically depends on the selected cooperation scheme. For example, joint transmission and/or reception in CoMP networks require precise phase synchronization among BSs. It can be realized either by central processing unit with remote radio heads (RRHs) [26] or by sharing a common carrier among BSs via optical fibers. However, it significantly increases the development cost, and also limits the flexibility to evaluate various measurement environments.

2.1.2 Multi-dimensional MIMO Channel Sounder

Multi-dimensional channel sounders [20] focus on the investigation of physical radio propagation mechanisms. Fully-switched array architecture that has a single radio front-end at both sides of Tx and Rx has been widely employed (e.g. [16, 21, 22, 23]) due to its cost-effectiveness, simple hardware implementation and easy calibration [24]. Such systems realize the double-directional analysis of propagation channel [25], but are mainly designed for the point-to-point MIMO channel characterization due to the difficulty in synchronization among multiple links. Also in the fully-switching architecture, temporal channel acquisition rate is usually limited by the time for array switching, hence the measurable maximum Doppler frequency will be restricted.

2.1.3 Multi-link Channel Sounding Techniques

A channel sounder for the double-directional channel investigations of multiple links was reported in [15]. The system is composed of two individually developed fully-switching MIMO channel sounders (single Tx and two Rxs). Frequency synchronization is achieved by a highly stable atomic oscillator which is used as the reference for local oscillators (LO) at each of the distributed devices. Array switching sequences are not synchronized since two Rxs are individually designed. This timing offset at two Rxs can be esti-

mated and removed in post-processing thanks to the same switching periods at Rxs (both of Rxs have same elements of array). Although its capability in estimating directional channel both at Tx and Rx with high resolution is valuable, the single Tx dual-link scenario will not be enough to cover a large variety of multi-link scenarios including MU-MIMO (i.e. distributed UEs) and CoMP (distributed BSs) networks.

Several multi-link channel measurement techniques have also been proposed as summarized in [11] for some limited measurement scenarios. In [31] and [32], multi-link channel measurements were realized based on a single sounder distributed antenna technique. In this method, frequency and phase synchronization can be achieved by connecting multiple antenna arrays to single MIMO sounder via RF cables. However, the measurement range is restricted by the loss in RF cables, so the applicable measurement scenarios are limited.

2.2 Design Considerations for Multi-link MIMO Channel Sounder

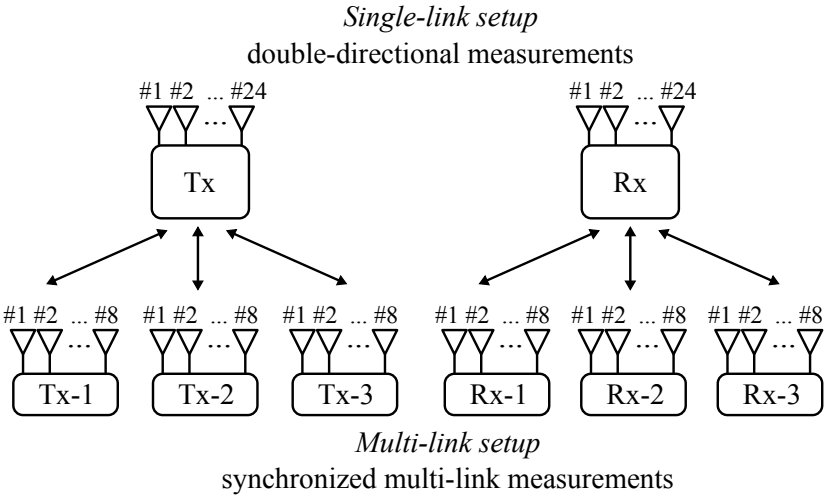

Figure 2.1 Scalable architecture for double-directional and multi-link measurements.

2.2.1 Choice of Hardware Architecture

The problem identified through the review of prior studies was that existing systems focus either on transmission aspect or on propagation aspect only. However at higher operating frequency, inter-relation of transmission performance and physical propagation phenomena need to be investigated in detail. For this reason, fully-parallel MIMO architecture was adopted for the channel sounder developed in this thesis. In parallel architecture, hardware calibration have to be carefully conducted to obtain the accurate channel estimates. Also there is two important practical issues that are not requisite in transmission system as follows.

1. Precise synchronization between Tx and Rx
   This is to estimate the absolute propagation delay and also for the directional estimation, precise synchronization is required in channel sounder. This is not the case in transmission system where delay due to the propagation channel is not the parameter of interest, hence the influence can be compensated using know training signals.

2. Back-to-back calibration
   This is to remove the influence of system hardware from measured channel. Back-to-back calibration becomes significantly difficult in fully-parallel architecture since all the combination of Tx-Rx RF port pairs must be connected one-by-one.

Despite its huge hardware complexity, the use of fully-parallel architecture realize the flexibility in evaluation of various multi-link MIMO scenarios. Accordingly, scalable modular-based channel sounder architecture is proposed as shown in Figure 2.1.

2.2.2 Choice of Synchronization Method

As briefly described in Sect. 1.1, the level of required synchronization depends on the channel parameters to be measured. Basically, precise synchronization in time and frequency are essential in any channel sounder for the estimation of absolute propagation delay and accurate TF estimation processing, respectively. It can be simply realized by using a highly stable atomic oscillator as reference for system clocks and RF carriers at separated devices. Although the phase-synchronized setup provides best accuracy in estimated TF neglecting the influence of system PN by sharing common LO or distributed antenna technique, it is not realistic in channel sounders where various measurement scenarios have to be investigated. In this regard, optimal synchronization setups for multi-link and directional measurements are proposed as follows. Schematics of synchronization setups are shown in Fig. 2.2.

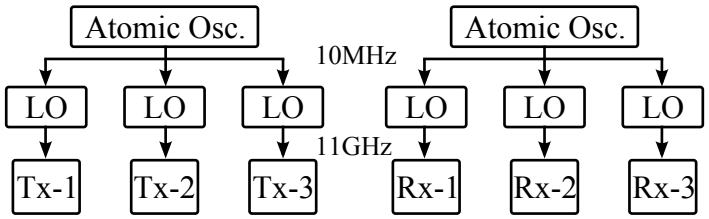

(a) Multi-link measurement

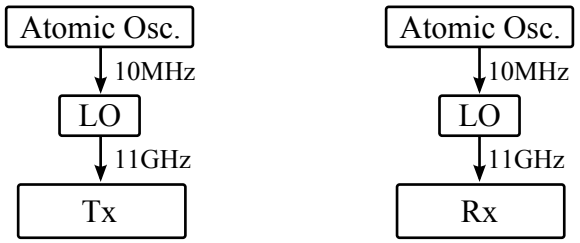

(b) Directional measurement

Figure 2.2 Synchronization setups for multi-link and directional measurements.

- Multi-link measurement setup [Fig. 2.2(a)]
  To enable the spatial separation of multiple Txs and Rxs, each of the casings needs to own individual LO while the reference signal from atomic oscillator can be shared within transmit or receive system since cable loss at 10 MHz can be negligible. Since directional estimation is not considered in this setup, the requirements on LO in terms of PN performance can be relaxed although the error in Doppler estimation is inevitable. Instead, multiple LOs within transmit or receive system should have comparable PN performances to minimize the influence of system PN imbalance which result in different TF estimation qualities at multiple casings.

- Directional measurement setup [Fig. 2.2(b)]

For the double-directional measurement, precise phase synchronization is required both at Tx and Rx. Since PN can be one of a major source of directional estimation error as reported in [39], high-precision LO is desired in this setup. Particularly the characteristics of PN should be analyzed in terms of standard deviation and phase drift during the symbol length to be processed. It should be noted that required level of synchronization in the directional setup corresponds to the joint processing in CoMP network. However, phase drift compensation technique which is commonly used in data transmission systems can not be applied in channel sounding since it is impossible to distinguish between phase drifts due to the propagation channel and phase drifts due to the system PN.

When considering the whole measurement duration of about several hours, system clock phases at transmit and receive systems may also shift due to the slight frequency offset between separated reference sources. The influence should be evaluated in terms of error in estimated absolute delay.

2.2.3 Scalable Sounder based on Fully-Parallel Architecture

To measure $N_{\mathrm{rx}} \times N_{\mathrm{tx}}$ MIMO channel matrix, multiplexing techniques are utilized to separate all transmitted signals from multiple antennas at receiver side. Basically, TDM (time division multiplexing), FDM (frequency division multiplexing) and CDM (code division multiplexing) schemes can be appropriately chosen depending on the system architecture. In this thesis,t o realize the scalability in probing symbol for MIMO channel TF estimation, FDM-STDM layered multiplexing proposed in [37] was implemented. The designed sounding parameters and resulting capabilities are summarized in Table 2.1, together with the symbol notations used throughout this paper. Fig. 2.3 shows the structure of probing signal frame which provides the single set of $N_{\mathrm{rx}} \times N_{\mathrm{tx}}$ MIMO channel matrix estimates (commonly called as *snapshot*).

Table 2.1 Sounding Parameters and Resulting Capabilities

System configuration	
No. antennas/casing ($2N_{\mathrm{A}}$)	8
No. Tx casings ($N_{\mathrm{U_{tx}}}/2$)	1, 2, 3
No. Rx casings ($N_{\mathrm{U_{rx}}}/2$)	1, 2, 3
No. Tx antennas (N_{tx})	8, 16, 24
No. Rx antennas (N_{rx})	8, 16, 24
Probing signal parameters	**(unit symbol)**
Waveform	Wideband multitone (with Newman phase [37])
No. FFT points (N_f)	4096
No. multitones (N)	2048
Signal bandwidth ($2B$)	400 MHz
Tone separation (Δ_F)	195.31 kHz
Frame format	
Symbol length (T_{sym})	5.12 μs
GI length (T_{GI})	1 μs
FDM order ($= N_{\mathrm{A}}$)	4
TDM order ($= N_{\mathrm{U_{tx}}}$)	6
FDM frequency shift (Δ_f)	48.83 kHz
Frame length (T_{frame})	† 48.96, 97.92, 146.88μs
Sounder capabilities	
Time delay resolution ($= 1/2B$)	2.5 ns
Max. delay ($\tau_{\max}$)	5.12 μs
Max. Doppler freq. ($f_{\mathrm{D,max}}$)	† 10.21, 5.11, 3.40 kHz
	† for $N_{\mathrm{tx}} = 8,\ 16,\ 24$

Multitone signal is often used to measure the channel response over a wide frequency range. Similarly to orthogonal frequency division multiplexing (OFDM), multi-tone signal is advantageous over the single carrier pseudo random sequence from the viewpoint of the spectrum efficiency although peak-to-average power ratio (PAPR) is higher. A method to minimize PAPR of multitone signals by introducing the Newman phase condition was proposed in [37]. The complex baseband multitone signal with Newman phase is given by

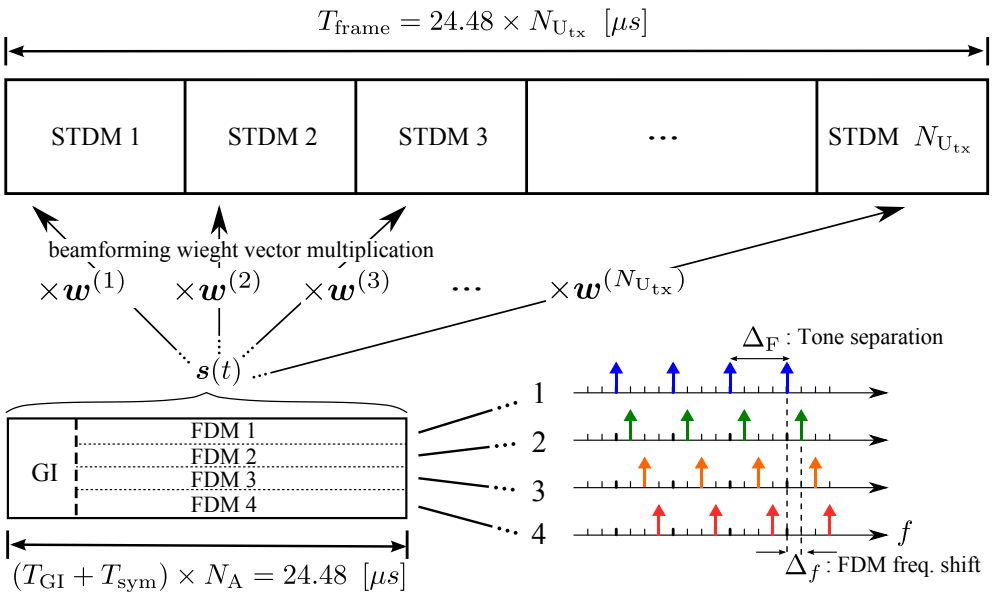

Figure 2.3 Frame format based on the FDM-STDM layered multiplexing.

$$m(t) = \frac{1}{\sqrt{N}} \sum_{n=0}^{N-1} \exp(j2\pi n \Delta_F t + j\varphi(n)) \tag{2.1}$$

where n and $\varphi(n) = n^2\pi/N$ are the frequency and Newman phase of the n-th tone, respectively. N is the number of tones to be allocated over the given frequency band and Δ_F is the carrier spacing. Multitone signal of (1) is frequency shifted for the amount of $\Delta_f = \Delta_F/N_{\text{A}}$ to ensure the orthogonality among tones. Resulting sounding symbol for the k-th FDM channel is represented following and transmitted from the k-th Tx antenna.

$$s^{(k)}(t) = m(t) \exp(j2\pi(k-1)\Delta_f), \quad k = 1, \cdots, N_{\text{A}} \tag{2.2}$$

For the multi-link measurement, STDM technique by transmit beamforming is also utilized. One STDM symbol consists of multitone signal with the length equal to the inverse of the FDM tone separation Δ_F. The beamforming weighted sounding symbols are represented by

$$\boldsymbol{x}_n^{(k)}(t) = \boldsymbol{w}_n \boldsymbol{s}^{(k)}(t) \tag{2.3}$$

where $\boldsymbol{w}_n \in \mathbb{C}^{N_{\mathrm{U_{tx}}} \times 1}$ is the transmit orthonormal beamforming weight vector for n-th TDM slot. On the other hand, the received signal for each of TDM slot can be represented in frequency domain as

$$\boldsymbol{Y}^{(k)}(f) = \boldsymbol{H}^{(k)}(f)\boldsymbol{W}(f)S^{(k)}(f) + \boldsymbol{N}(f) \tag{2.4}$$

where $\boldsymbol{W}(f)$, $S^{(k)}(f)$ and $\boldsymbol{N}(f)$ denote the Fourier transforms of the weighting vector, FDM symbol $s^{(k)}(t)$ and white Gaussian noise process $\boldsymbol{n}$(t). Single FDM symbol can be obtained by $\acute{\boldsymbol{Y}}(f) = \acute{\boldsymbol{Y}}^{\ (k)}(f)\ \boldsymbol{W}^{-1}$. Here, the received signal $\tilde{\boldsymbol{Y}}(f)$ contains all the subcarrier components mixed through propagation channel. By using known transmitted FDM signal $\boldsymbol{X}^{(k)}(f)$, channel matrix can be estimated by

$$\tilde{\boldsymbol{H}}(f) = \tilde{\boldsymbol{Y}}(f)\boldsymbol{X}^{(k)}(f)^{\mathrm{H}} \tag{2.5}$$

where ^{H} denotes the complex conjugate operator. Note that the estimated channel matrix of $\tilde{\boldsymbol{H}}(f)$ includes the characteristics of measurement system, and it can be removed by calibration process described in latter chapter.

Four transmitting signals within the same unit are multiplexed by FDM and then the signals of the same FDM channel from six different units are generated by orthogonal beamforming over six consecutive symbols. The STDM provides the additional processing gain compared with conventional TDM method in fully-switching architecture. Although the probing signal format can be scalable in units of 4, a single casing of the actual developed system consists of 8 RF ports for convenience in hardware realization. Accordingly, the resulting frame length for the 24 Txs configuration becomes $T_{\mathrm{frame}} = 146.88\ \mu$s. The frame length T_{frame} determines the maximum Doppler frequency can be estimated from the continuous measurement, since its inverse $f_{\mathrm{rep}} = 1/T_{\mathrm{frame}}$ corresponds to the channel sampling rate in the real-time t-domain. To satisfy the sampling theorem to avoid aliasing, the Doppler frequency can be managed becomes

$$f_{\mathrm{D}} < \frac{1}{2} f_{\mathrm{rep}} \tag{2.6}$$

Hence, maximum Doppler frequency of $1/2T_{\mathrm{frame}} = 3.40$ kHz can be managed.

2.3 Summary

In this chapter, a scalable channel sounding technique was described based on the review of existing studies. The use of fully-parallel MIMO architecture realize the flexibility for directional measurement by combining casings and for multi-link MIMO measurement by separating casings. The flexibility allows the the evaluation of various multi-link scenarios with knowledge of physical propagation mechanism that is beneficial for understanding observed multi-link MIMO transmission performance and channel modeling.

A scalable multiplexing scheme based on the FDM-STDM hybrid multiplexing was also described. In this scheme, measurable Doppler frequency shift of 3.4 kHz is achieved thanks to the parallel architecture. This is high enough to investigate time-variant radio channel even at 11 GHz frequency band. However in a practical system, continuous signal acquisition is limited to about 1.3 seconds with current memory capacity. This is because the fast sampling rate of 800 MHz at each of 24 parallel receiver chains. In this regard, time-grid acquisition is implemented, and the detail is described in the next Chapter.

Chapter 3

System Implementation

3.1 Introduction

This chapter presents the implementation of scalable channel sounder designed in previous chapter. The schematic diagram of the overall system is shown in Fig. 3.1. Each Tx and Rx system is composed of 3 casings with 8 RF ports, laptop PC for casing control and Cesium frequency standard for synchronization. System control and TF estimation processing were implemented in C language. The remote laptop PCs can connect to the CPU of each casing via Ethernet/WiFi network for setting up the sounding parameters and checking estimated results on site. The details of the developed system is described in the following sections.

3.2 Choice of Frequency Reference Source

The performances of the frequency reference source and the LO are the fundamental element in channel sounder design. The principle of the synchronization is shown in 3.2. Frequency offset between Tx and Rx causes long-term phase drift, thus limiting the estimation accuracy in Doppler frequency shift and absolute delay of propagation paths. The required accuracy and stability

of the frequency reference should be determined by the resulting frequency offset in 11 GHz carrier frequency, since every LO is driven by a 10 MHz output of a reference oscillator. Here, the performance of Rubidium [40] and Cesium [41] oscillators are compared among commercially available products. As shown in Tab. 3.1, the typical performances of Rubidium and Cesium frequency standards are in order of 10^{-11} and 10^{-13} in frequency accuracy (with consideration of stability within < 100 s) and resulting phase drift at 11 GHz can be calculated as $36°/s$ and $0.36°/s$, respectively. It is clear that even without considering the influence of PN at LO, the use of Rubidium results in significant phase drift at 11 GHz. Accordingly, Cesium frequency standard was selected in the developed channel sounder. It enables the complete separation of Tx and Rx systems with acceptable system phase drift, and realize the flexibility in measurement including outdoor large scale scenarios.

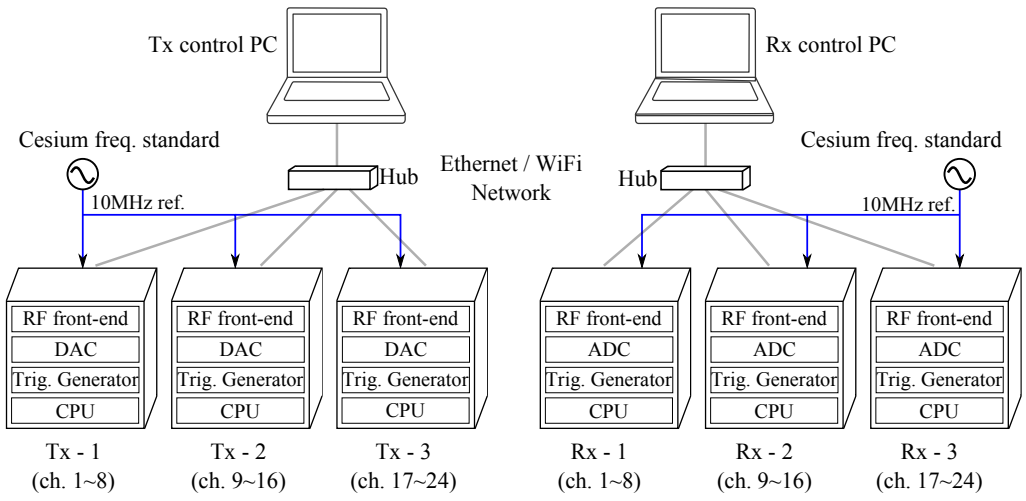

Figure 3.1 Schematic diagram of 24×24 scalable MIMO channel sounder.

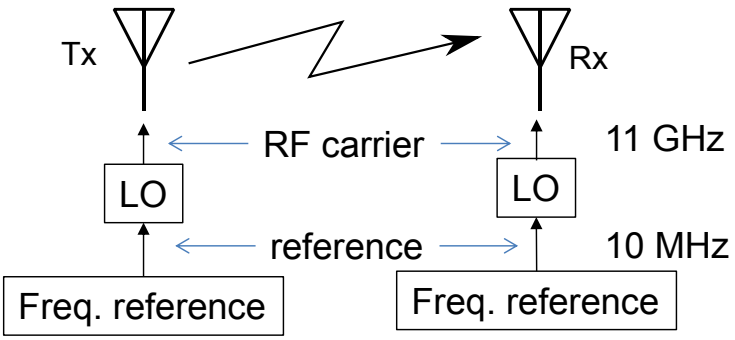

Figure 3.2 Synchronization principle of general channl sounder.

Table 3.1 Performance of the commercially available frequency standard.

	Precision at 10 MHz	Phase drift at 11 GHz
Rubidium [40]	$\pm 1.0 \times 10\text{E}{-11}$ Hz	36 deg./sec.
Cesium [41]	$\pm 1.0 \times 10\text{E}{-13}$ Hz	0.36 deg./sec.

3.3 System Implementation

3.3.1 Developed Hardware Components

3.3.1.1 8×8 MIMO Channel Sounder

Each of the Tx and Rx casings that consists of 8 parallel transmit or receive chains, respectively, was implemented based on the generic software defined radio (SDR) platform [42]. The platform is also utilized as a 8×8 MIMO-OFDM experimental system in [47]. Fundamental specifications of the 8×8 MIMO channel sounder are summarized in Table 3.2. Figs. 3.3 and 3.4 are the block diagrams and photos of the casing, respectively. The whole system is composed of three sets of 8×8 MIMO channel sounders.

Table 3.2 System Specifications

Base platform (TD-SPP3000 [42])	
Casing	CompactPCI (6U)
No. slots	10
Baseband Circuit	
Sampling rate	800 MHz
FPGA (Xilinx Inc.)	Virtex-5 VLX110T [43]
DAC (Texas Instruments Inc.)	16 bit, 1 GSPS (DAC5682 [44])
ADC (Texas Instruments Inc.)	12 bit, 1 GSPS (ADS5400 [45])
Delay chip (ON Semiconductor)	10 ps step (MC10EP195 [46])
Waveform memory	1 G samples / channel
RF Front-end	
Architecture	direct-conversion
Center frequency	11 GHz
Cut off freq. at LPF	250 MHz
Transmit power / ant.	10 mW
PA gain	$-3 \sim +17$ dB (Tx)
	$+33 \sim +57$ dB (Rx)

The casing is based on a compact PCI (cPCI) standard [48], and ten 6U (160mm $\times$ 233 mm) cPCI boards can be packed in a single casing. A CPU board for transmit/receive processing, clock-trigger board for sampling clock and trigger pulse generation, four DAC/ADC boards and two RF up/down converter boards are installed in a Tx/Rx casing, respectively. All the system clocks within the casing are generated from the 10 MHz reference signal from the external Cesium oscillator for synchronization. An 11 GHz carrier can be generated at each casing by an internal synthesizer module. However due to the space limitation, PN performance of the internal LO could not be so high (-60 dBc/Hz @ 1 kHz offset), and its influence on TF estimation accuracy was identified as significant. To avoid this issue, an external high-precision LO was developed based on the design guidelines proposed in [37]. The detailed PN performance of the developed LOs is presented in Chapter 4..

The trigger pulses synchronize transmission and reception timing of sound-

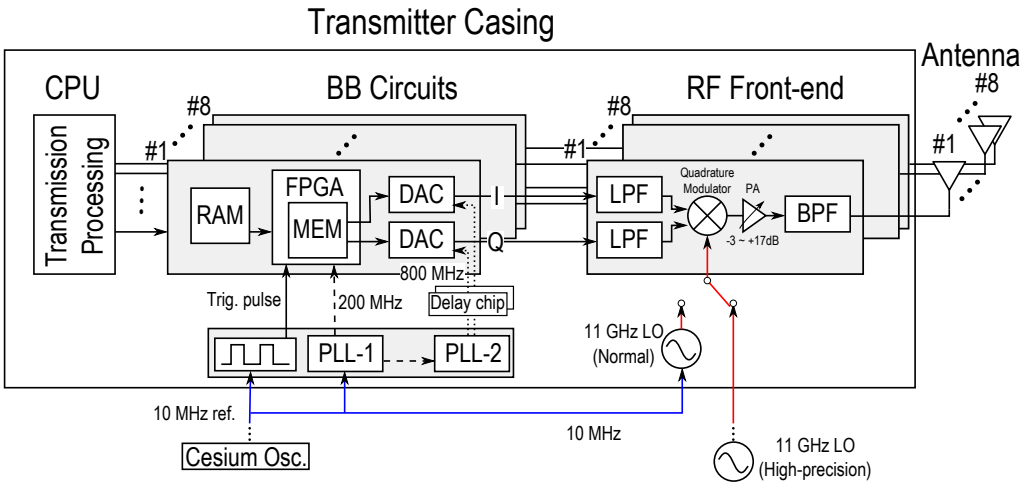

(a) 8 channels Tx casing

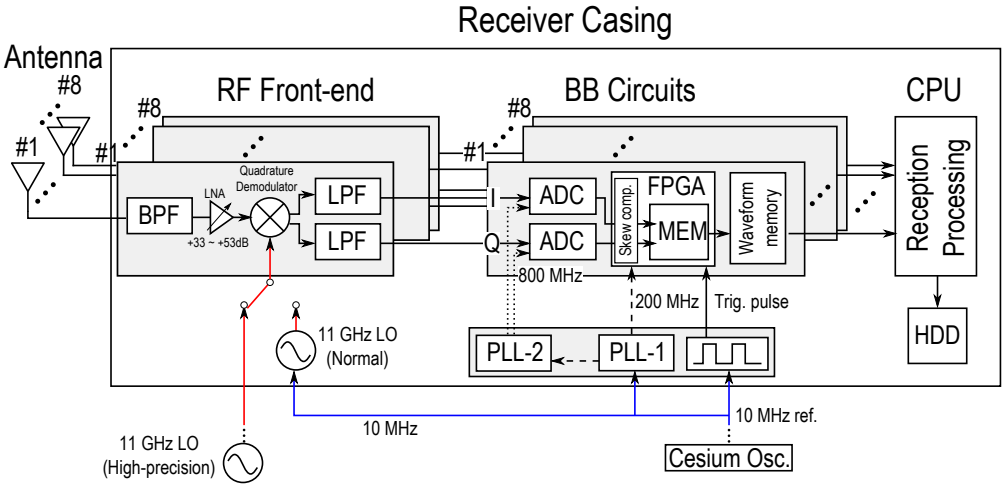

(b) 8 channels Rx casing

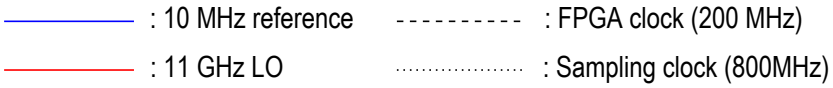

Figure 3.3 Block diagrams of single casing based on a generic SDR platform. (External Cesium oscillator and high-precision LO are also shown together)

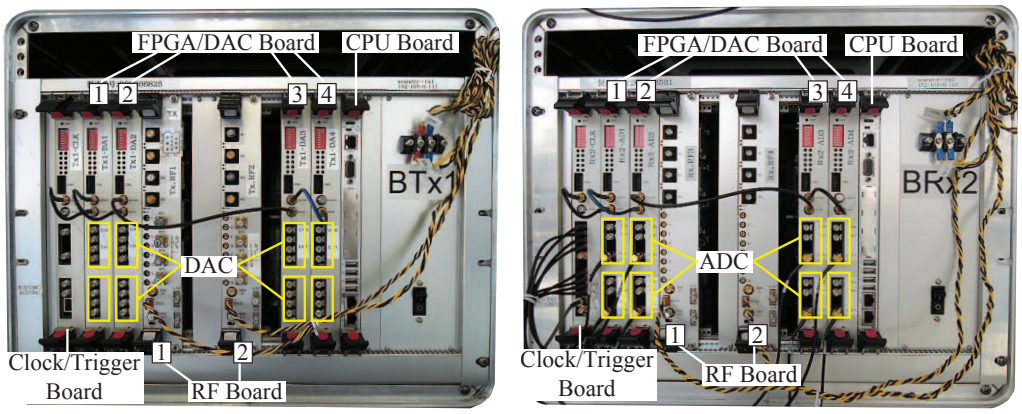

(a) 8 channels Tx casing. (b) 8 channels Rx casing.

Figure 3.4 Photos of single casing for (a) Tx and (b) Rx.

ing frames. All the trigger pulses at 3 Tx and 3 Rx casings are first synchronized during the calibration process automatically by connecting each other via cables. Trigger pulse synchronization can be maintained within the stability of reference signal from Cesium oscillator, and actual synchronization performance and its impact on channel sounding is evaluated in the performance evaluation section in Chapter 4. The FPGA on the DAC/ADC board serves as the interface among peripheral circuits (i.e. DAC/ADC, waveform memory and PCI bus), and transmission and reception are processed at the CPU. Programmable delay chips can control the 800 MHz sampling clocks with 10 ps precision, and calibrate the timing mismatch (skew) of outputs from DACs and ADCs. At the Rx casings, each receive chain is equipped with memory as temporary storage for the received waveforms.

As for the RF analog front-end, both of the quadrature up and down-converters are developed based on a direct-conversion architecture due to the advantages in low-cost and small-size implementation. However, the direct-conversion architecture is usually sensitive to the IQI and carrier leakage problems [49], and digital compensation is necessary. Details of the implemented technique is described in Chapter 4.

3.3.1.2 Antenna Array

Two types of antennas were developed for two purposes, directional measurements (Fig. 3.5) and MIMO performance evaluation (Fig. 3.6). Both of the antennas are composed of dual-polarized (vertical and horizontal) elements so that polarized MIMO channel behavior could be measured. The complex spherical radiation patterns of 12-elements uniform circular array (UCA) was carefully measured in an anechoic chamber to enable the directional estimation by means of beamforming and maximum likelihood parameter estimation. The angular resolution of the UCA is about 23 ° as shown in Fig. 3.7 which is defined as the half-power beam width (HPBW) calculated when the every elements were assumed as omni-directional and beam forming is applied into 0 ° direction. The radiation pattern of the single element of the UCA measured in an anechoic chamber is also shown in Fig. 3.8 for each of the polarization pairs. For the MIMO performance evaluation, an omni-directional sleeve antenna (4 dBi) and sector antenna (15 dBi) with HPBW of 65° can be selected to compose antenna array in Fig. 3.6. The orientation and inter-element spacing can be flexibly changed for the evaluation of MIMO performance in various antenna configurations.

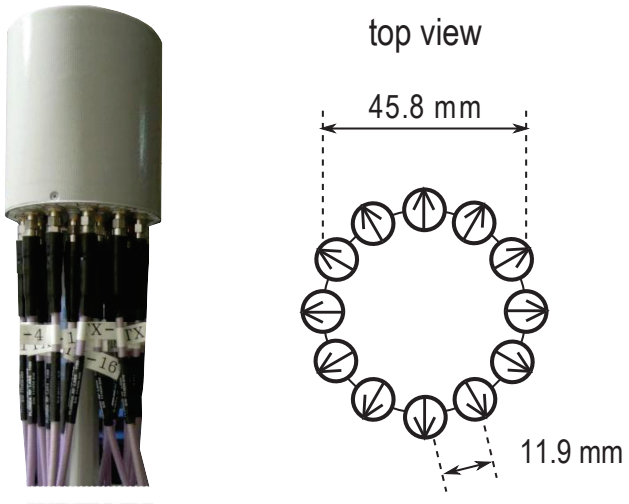

Figure 3.5 12 elements dual polarized circular array for directional estimation.

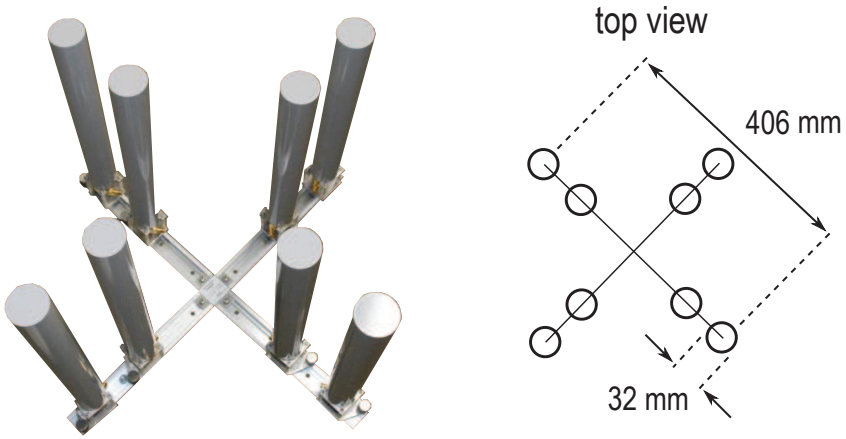

Figure 3.6 Dual-polarized antennas for MIMO performance evaluation. (8 elements example configuration is shown)

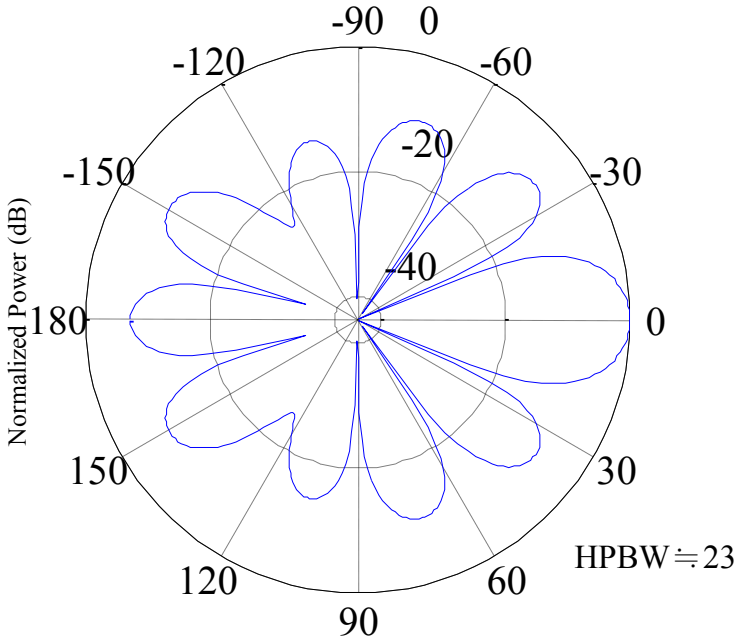

Figure 3.7 Simulated angular resolution of the 12-elements UCA.

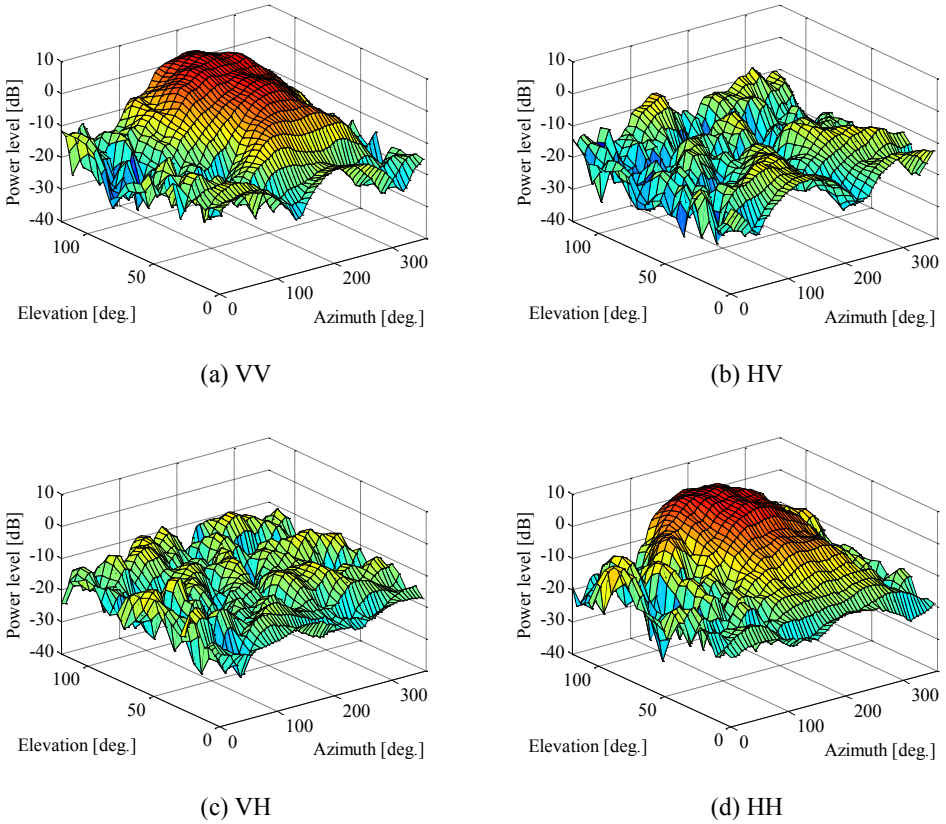

(a) VV (b) HV

(c) VH (d) HH

Figure 3.8 Radiation pattern of the 12-elements UCA measured in an anechoic chamber (8th element). The order of the notation: element at Rx, element at Tx. i.e. VH: horizontal polarization at Tx, vertical polarization at Rx.

3.3.2 Time-Grid Data Acquisition

Due to the ADC's fast sampling rates, possible continuous measurement duration is limited to about 1.3 seconds with current memory capacity. For the block-wise storage of the consecutive snapshots into the memory in regular interval, time-grid data acquisition is implemented as shown in Fig. 3.9. In this scheme, the data acquisition mode at Rx is specified by block interval T_{b} and the number of consecutive snapshots in single block period, N_{s}. The block interval T_{b} can be selected within the range $5 \times T_{\mathrm{frame}} \times 2^{0,1,\cdots,10}$ (0.73 ms $\sim$ 0.75 sec. in case of $N_{\mathrm{tx}} = 24$) considering the expected maximum

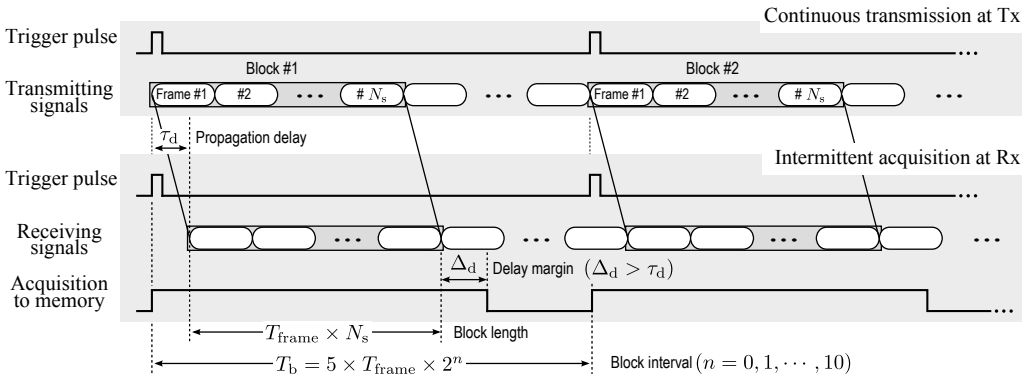

Figure 3.9 Synchronized data acquisition and time-grid principle. The data acquisition mode at Rx is specified by block interval T_b and the number of consecutive snapshots in single block period, N_s.

Doppler frequency in the environments. The number of continuous snapshots N_s is selected depending on the necessary continuous measurement duration and averaging gain of $10 \times \log 10(N_s)$ for signal-to-noise-power-ratio (SNR) enhancement.

3.4 Calibration

This section presents the calibration techniques for the developed MIMO channel sounder. The system calibration aimed at measuring the TFs of the system hardware accurately across the sounding bandwidth (commonly called as *back-to-back calibration*), so that the system characteristics can be removed from channel TFs obtained by propagation measurements. However, each parallel hardware chain suffers from IQI in terms of phase, amplitude and DC offset, which degrades the accuracy in channel TF estimation [37]. Therefore, such hardware impairments must be compensated prior to the back-to-back calibration. Also in the fully-parallel MIMO architecture, all the TFs of Tx-Rx RF port pairs (i.e. $24 \times 24 = 576$) need to be measured

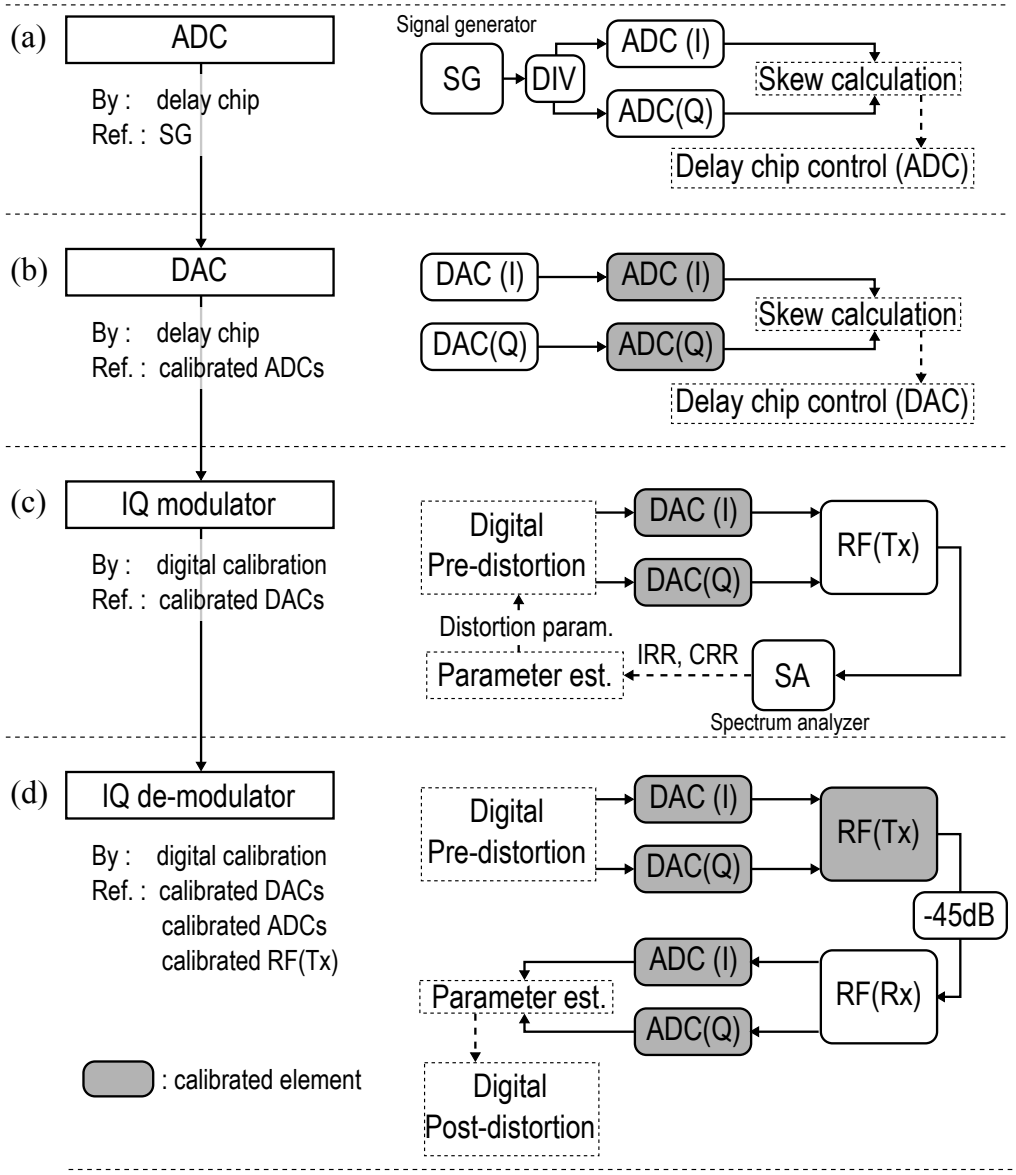

Figure 3.10 Calibration procedure and corresponding block diagrams.

in back-to-back calibration whenever the system is turned on. For these purposes, several calibration techniques were implemented as described in the following subsections.

3.4.1 Calibration Procedure

Effects of hardware impairments in the FDM-STDM layered multiplexing sounder was evaluated in [37] by means of computer simulation. The normalized mean square error (NMSE) was used as a metric of estimation accuracy defined as

$$\mathrm{NMSE} = \frac{\sum_k \left| \hat{H}[k] - H[k] \right|^2}{\sum_k |H[k]|^2}, \tag{3.1}$$

where $\hat{H}[k]$ and $H[k]$ are the estimated TF and simulated known TF for multitone index k, respectively. The square root of NMSE corresponds to the error vector magnitude (EVM) which is widely used as a quality measure of transmission systems [50], namely NMSE = $(\mathrm{EVM})^2$. Basically, the effects of IQI are observed as mirror image distortion and carrier leakage in the frequency domain. The influence of carrier leakage can be easily compensated in post-processing by replacing the center frequency tone with the mean of neighboring tones. On the other hand, the mirror image components cause interference between FDM tones, and degrade the system performance. Accordingly, the image rejection ratio (IRR) [51] that is defined as the relative level of image tone against the fundamental tone is appropriate to evaluate the effects of IQI. The desired compensation level proposed in [37] was -40 dB in IRR at both Tx and Rx, and was adopted as the compensation requirement in this study. This threshold results in an NMSE of approximately 2.0×10^{-4} (equivalent EVM of 1.4%) in case of single-input-single-output test measurement with no influence of PN.

Although the evaluation in [37] considered IQI in the RF front-end only, the same criteria can be applied in the actual hardware since the errors in

measured TFs are observed as a combined effect. However, compensation has to be conducted individually for baseband and RF circuits due to the difference in stability. Basically, the IQI in the baseband circuits are relatively stable. On the other hand, IQI in the RF front-end is sensitive to the temperature of surrounding environment and heat-run condition. In this regard, compensation was first applied to the baseband circuits using programmable delay chip, then IQI in the RF front-end was compensated by means of digital pre-/post-distortion techniques at Tx and Rx, respectively. Fig. 3.10 shows the flow of hardware impairments compensation and their corresponding block diagrams.

3.4.2 Baseband Circuit Tuning

The block diagrams for baseband compensation at ADCs and DACs are shown in Fig. 3.10(a) and 3.10(b), respectively. A programmable delay chip [46] can be used to delay the sampling clock for DACs with precision of 10 ps. However in the Rx baseband board, the delay chip could not be installed due to some limitation in hardware structure. For this reason, a digital interpolation filter was implemented in the FPGA which can adjust the delay of ADC output signals with 10 ps resolution. The skew in the ADC IQ chains was first compensated by referring to a 25 MHz single tone from a signal generator (SG), assuming frequency independent IQI. The delay chip was controlled by the FPGA based on the measured IQ skew in output signals from ADCs. The skew in DACs can be compensated in same way as ADCs but calibrated ADCs. As a result, baseband IQ skew of < 50 ps, which corresponds to $\sim 5 \times 10^{-5}$ of NMSE, could be achieved through compensation at both DACs and ADCs.

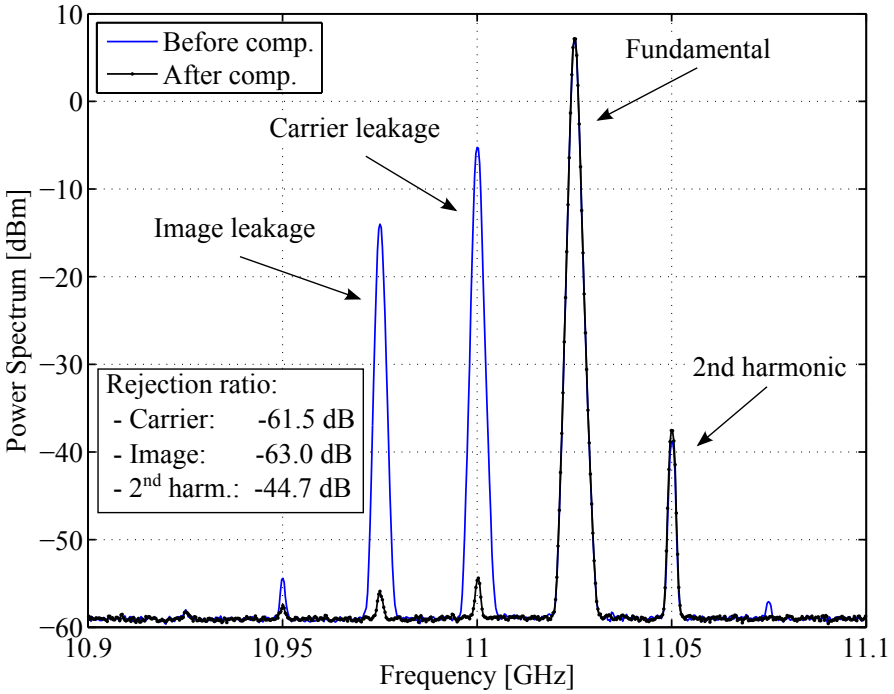

Figure 3.11 The effect of IQI compensation at quadrature modulator.

3.4.3 IQ Imbalance Compensation for RF Imperfections

For the compensation of IQI at the quadrature modulator, digital pre-distortion technique was utilized based on the method proposed in [38, 52]. In this method, IQI model parameters (phase and amplitude mismatches and DC offsets at IQ branches) need to be accurately estimated to determine the coefficients for pre-distortion processing. A feedback loop system for the parameter estimation was realized using the Ethernet interface of a spectrum analyzer (SA, FSU43, Rohde&Schwarz) as shown in Fig. 3.10(c). IRR and carrier rejection ratio (CRR) measured by the SA are sent to the CPU of the Tx casing, and IQI model parameters can be estimated. The result of IQI compensation at the quadrature modulator is shown in Fig. 3.11 when a 25 MHz exponential tone is used as test signal. As a result, both

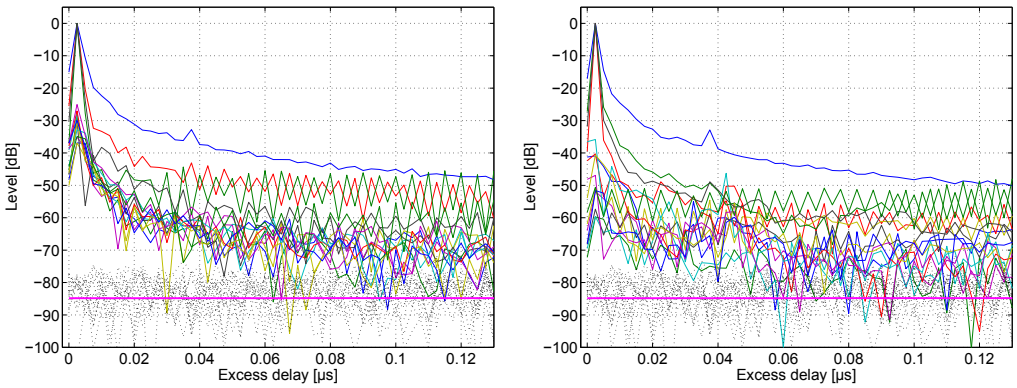

(a) Before IQ compensation. (b) After IQ compensation.

Figure 3.12 Channel impulse responses measured by back-to-back before and after applying IQ compensation.

the IRR and CRR were sufficiently suppressed below the threshold level of −40 dB. It should be noted that relatively large second harmonic component was observed in the developed up-converter module, and it could not be compensated using the current method. However, influence of the harmonic component is sufficiently small since its rejection ratio is still below the desired threshold level.

Compensation of the quadrature de-modulator IQI can be conducted much more easily as shown in Fig. 3.10(d), since all the other circuit elements were already calibrated and down-converted digital signals can be used to calculate the IQI model parameters. The obtained parameters were used for digital post-distortion to eliminate the IQI at quadrature de-modulator.

3.4.4 Back-to-back System Calibration

n order to remove the transfer characteristic of the system itself from the measured channel, it is necessary to measure the TF of the system across the signal bandwidth. Basically in the fully-parallel MIMO architecture, all the

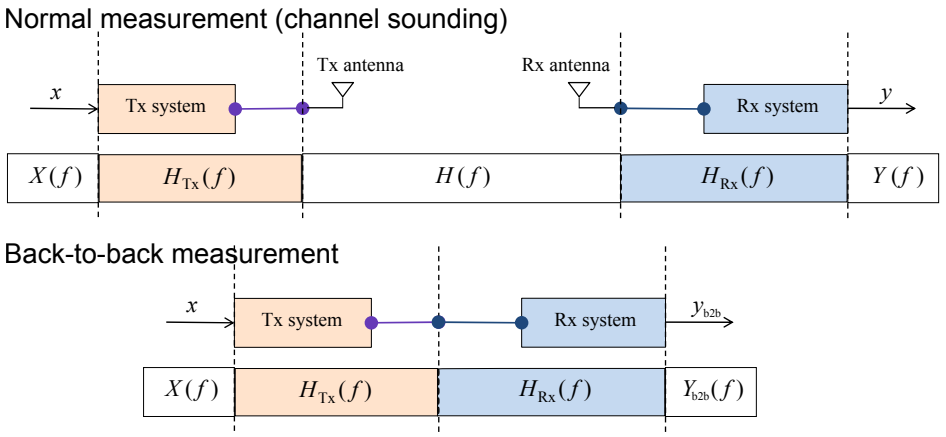

Figure 3.13 Concept of back-to-back calibration to remove the system characteristics from measured channel.

combinations of Tx-Rx RF ports need to be connected one by one via RF cable with known transfer characteristics to obtain the desired system TFs. This method is not realistic in the developed channel sounder which has 24 RF ports both at Tx and Rx since repetitive cable connections may cause loss in measurement accuracy. Moreover, calibration time needs to be short enough to avoid the effect of long-term phase drift in case the Tx and Rx systems are driven by individual reference signals.

For these reasons, a switching circuit which is equipped with 8 input/output ports and a -45 dB attenuator was developed as shown in Fig. 3.14. The input switching can be controlled from an external PC, hence 8×8 system TFs can be measured at once without any change in the physical setting. The influence of the switching circuit, whose transfer characteristics were measured beforehand by a vector network analyzer (VNA), can be removed from measured system TFs in post-processing. In this calibration method, total time for back-to-back calibration can be reduced to within 30 minutes which is short enough to avoid the long-term system phase drift.

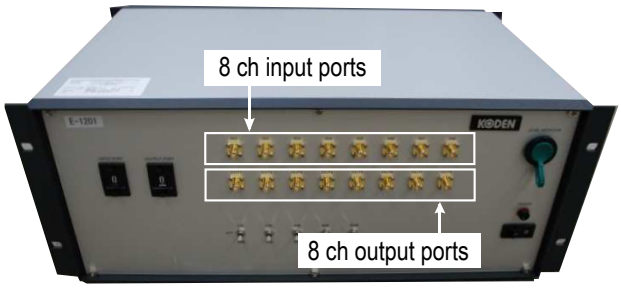

(a) Photo of 8×8 input switch circuit.

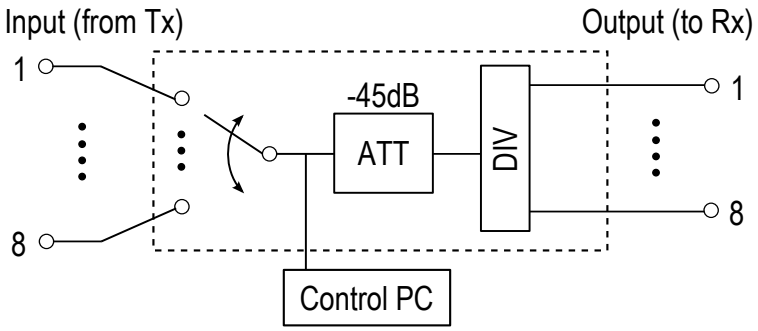

(b) Block diagram of 8×8 input switch circuit.

Figure 3.14 A 8×8 input switch circuit used for back-to-back calibration.

3.5 Summary

In this chapter, implementation of channel sounder based on the proposed fully-parallel MIMO architecture is presented. Also a time-grid measurement principle was proposed to avoid the problem in waveform memory size. The parameters of snapshot interval, number of continuous snapshot can be flexibly selected depending on the Doppler effect to be measured and snapshot averaging for the SNR improvement.

Several system calibration techniques that was identified as one of main issue in fully-parallel MIMO channel sounder was proposed. First, compensation techniques for hardware imperfection (IQ imbalance) is implemented

based on the required compensation accuracy identified through computer simulation. The effect of IQ imbalance compensation is confirmed by comparing the measured channel impulse response before and after the compensation. The positive effect was observed as the reduction in cross-talk between MIMO channels.

Finally, the simplified back-to-back calibration method using 8×8 switching circuit is proposed. The proposed method not only improve the accuracy of calibration, but also significantly reduce the time for calibration measurement to within 30 minutes. This is to avoid the influence of long-term system phase drift during the switching measurement across 24×24 MIMO hardware chains. Actual influence of system phase drift is evaluated in Chapter 4.

Chapter 4

Performance Evaluation

4.1 Influence of Separated Frequency References

As discussed in previous chapter, Cesium frequency standards were used to keep the synchronization among separated casings. Due to the excellent accuracy and stability ($\sim 10^{-13}$) of the Cesium standard, influence of center frequency offsets (CFO) can be negligible even at the 11 GHz frequency band [53]. However, actual channel sounding campaigns will take at least half a day. Therefore the influence of a slight frequency offset on channel sounding performance should be checked. For this purpose, trigger pulses at each of the casings, which are synchronized to 10 MHz reference signals from individual Cesium oscillators, were measured by oscilloscope for 12 hours. The measured trigger pulses and calculated offset values are plotted in Fig. 4.1(a) and 4.1(b), respectively. Observed linear increase in offset value is clearly the result of the frequency offset between separated frequency references. The slope of the pulse offset is about 0.77 ns/hour, which is within the range of the expected offset value based on the precision of Cesium oscillator. Considering the delay resolution of 2.5 ns and practical measurement duration of about 6 hours, the observed trigger pulse offset will cause ambiguity in estimated delay of

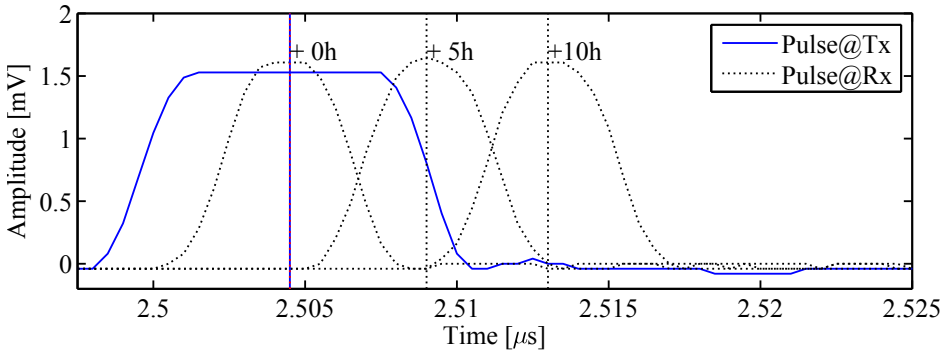

(a) Variation of trigger pulses at Rx casing against Tx pulse.

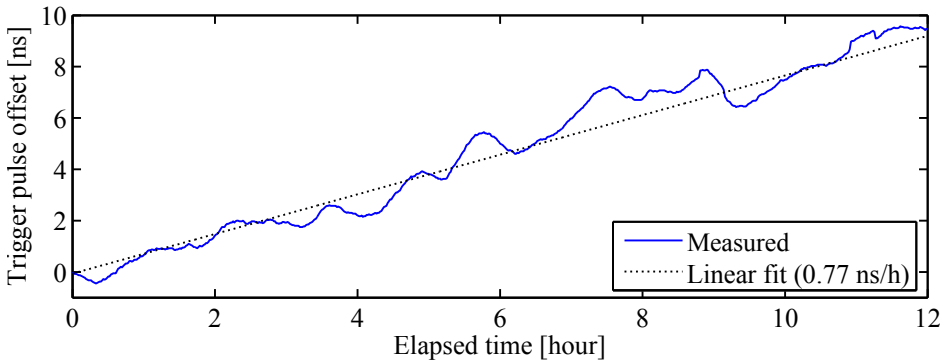

(b) Measured trigger pulse offset.

Figure 4.1 Trigger pulse offset due to frequency offsets between separated Cesium oscillators.

$\leq$ 7.5 ns. The results in Fig. 4.1 also confirmed that the about 30 min. time for back-to-back calibration based on the switching circuit is short enough to avoid the influence of separated frequency references.

4.2 Phase Noise

In the developed channel sounder, two types of LOs can be selected depending on the measurement setups. The LOs installed in every casing (internal LO) are used for the multi-link measurement, where the casings have to be

Table 4.1 SSB-PN Performances of Local Oscillators (Typical)

[dBc/Hz]	1 kHz	10 kHz	100 kHz	1 MHz
Internal LO (normal)	−60	−70	−100	−120
External LO (high-precision)	−103	−113	−119	−143

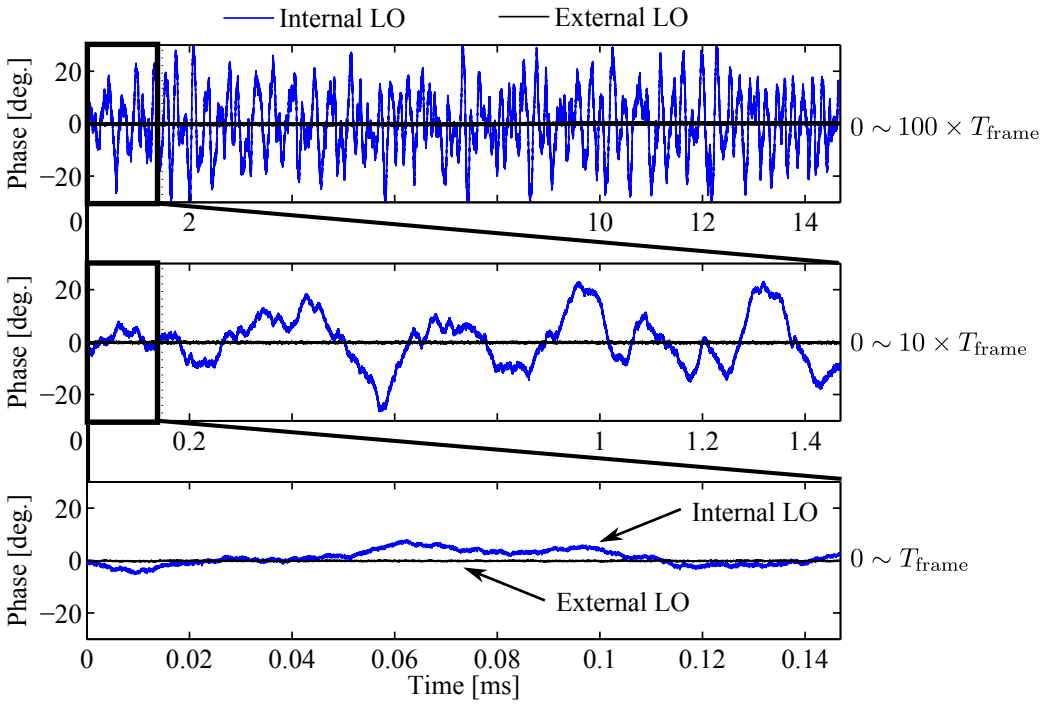

Figure 4.2 Variations of system phase noise.

separated from each other. Two external LOs for Tx and Rx sides can be used in the single-link directional measurement. Typical performance of the developed LOs are shown in Table 4.1 in terms of single-side-band phase

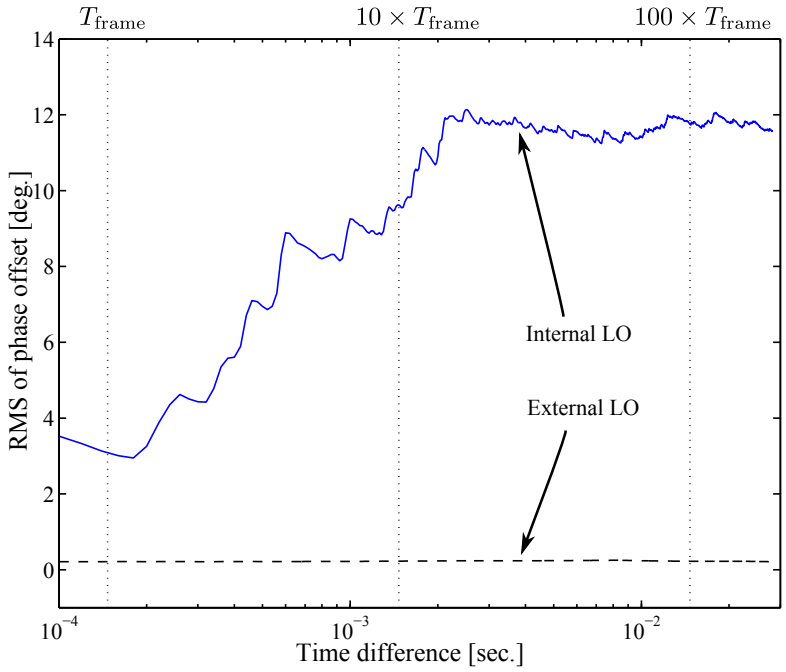

Figure 4.3 RMS value of phase offset.

noise (SSB-PN) spectrum. Influence of the PN on TF estimation accuracy was evaluated by computer simulation in [37] based on the two SSB-PN models which corresponds to the LOs used in the developed system (normal-precision internal LO and high-precision external LO). The paper concluded that the influence of PN in high-precision external LO is negligible, and effect of IQI dominates the channel sounder performance.

To confirm the actual PN performances, system PN was measured for two types of LOs. In the measurement, Tx and Rx RF ports were connected via cable and a -45 dB attenuator. The Tx and Rx casings were driven by individual reference sources from Cesium oscillators. Fig. 4.2 shows the phase variations during $0 \sim 100 \times T_{\text{frame}}$ (in case of $N_{\text{tx}} = 24$, $T_{\text{frame}} = 146.88$ μs). In this time range, there was no influence of separated reference sources since the long-term mean of the PNs were not drifting in both of the LOs.

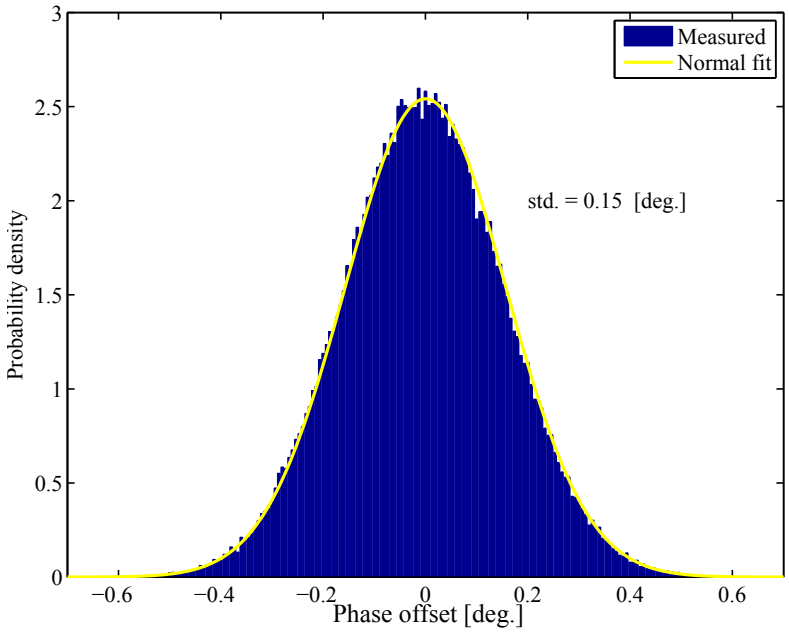

Figure 4.4 Probability density of phase offset within a frame length when external LOs are used both at Tx and Rx.

A random walk PN behavior was observed when internal LOs were used at both Tx and Rx. The root-mean-square (RMS) values of measured PNs were plotted in Fig. 4.3 for the quantitative evaluation. When internal LOs were used, the RMS value of phase offset was about 4° at a frame length and increased to about 12° at $100 \times T_{\text{frame}}$ duration. Influence of the observed phase fluctuations are not negligible, so the internal LO can not be used for the directional measurement where accuracy in estimated directional parameters is sensitive to the system PN effect [39]. However for the purpose of MIMO performance evaluation in multi-link measurement, the estimated multi-link channels are still comparable with each other since developed internal LOs have more of the same PN performance shown in Table 4.1.

On the other hand, the use of external LO results in very small fluctuations in system PN. The calculated RMS value in Fig. 4.3 was as small as 0.3° across the time duration of interest. Moreover, it was observed that the PN variation can be characterized by the white noise as confirmed by the probability density plot in Fig. 4.4. The standard deviation of the fitted

normal distribution was 0.15° which is small enough compared with PN performances of existing directional channel sounders (e.g. std. $\geq 3°$ in [15]). Therefore, it could be confirmed that the developed external LO can be used for the purpose of directional measurement.

Table 4.2 Link Budget Specifications and Measured Performance

Design specifications

Block	Parameter	Notation	Unit	Value	Accum.
Tx	Tx output power	P_{t}	dBm	10.0	10.0
	Cable loss	L_{cable}	dB	5.0	5.0
	Ant. gain (sector)	G_{t}	dBi	15.0	20.0
Rx	Ant. gain (sleeve)	G_{r}	dBi	4.0	24.0
	Cable loss	L_{cable}	dB	5.0	19.0
	Noise figure	NF	dB	8.0	11.0
	Processing gain [1]	G_{proc}	dB	13.8	24.8
	Required SNR [2]	SNR_0	dB	5.9	18.9
	Thermal noise [3]	N_0	dBm	−88.0	106.9
Allowed loss in air			dB	–	106.8
Allowed loss w/o ant. gain			dB	–	93.8

Measured performances

Allowed insertion loss	dB	93.1
Allowed loss in air	dB	106.2
Allowed meas. range in free-space	m	450

[1] in case of $N_{\mathrm{tx}} = 24$, $G_{\mathrm{proc}} = 10 \log_{10} N_{\mathrm{tx}}$.
[2] calculated so that the error in Rx output to be smaller than 1 dB.
[3] at temperature of 300 K, resistance of 50 Ω and 400 MHz bandwidth.

4.3 Receiver Sensitivity and Dynamic Performance

The dynamic performance of a channel sounder is basically characterized by the sensitivity level of Rx. The Rx sensitivity is determined by the noise figure (NF) in the RF front-end and quantization noise in the ADC, and such hardware specifications need to be carefully designed.

Table 4.2 shows the design specifications of link budget parameters and

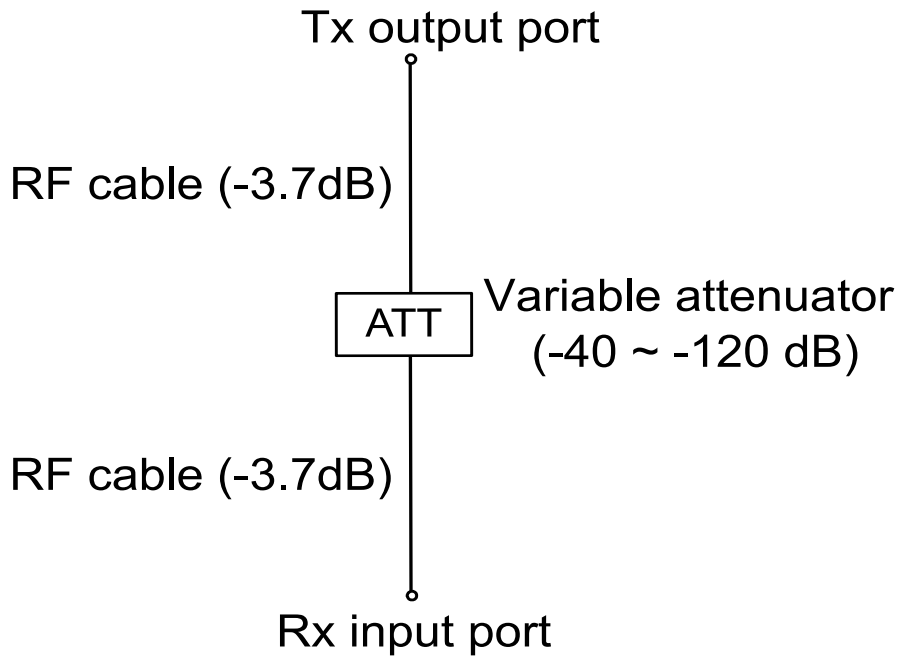

Figure 4.5 Schematic diagram of the measurement for the receiver sensitivity evaluation.

actual dynamic performance evaluated in back-to-back measurement. The developed channel sounder has no automatic gain control (AGC) functionality in Rx, but is equipped with variable low noise amplifier (LNA) whose gain can be manually controlled between $33 \sim 53$ dB. The value of NF in the table is for the case of 53 dB gain at LNA which corresponds to the worst case in Rx sensitivity. As a result, allowed propagation loss in design is 106.8 dB including antenna gains and processing gain due to STDM multiplexing.

To confirm the dynamic performance of the developed sounder, a back-to-back measurement was conducted by connecting Tx-Rx RF ports via RF cables with a variable attenuator inserted between them. The setup of the measurement is shown in Fig. 4.5. The results are shown in Fig. 4.6. The level of attenuator (L_{att}) was varied between $40 \sim 120$ dB. For the evaluation, wide-band path gain was calculated for different Rx port input power levels by summing all the absolute power of 2048 delay bins. The path gain is defined as the relative power level of measured channel impulse response (IR) which is calibrated by the IR at $L_{\mathrm{att}} = 45$ dB. The vertical axes on

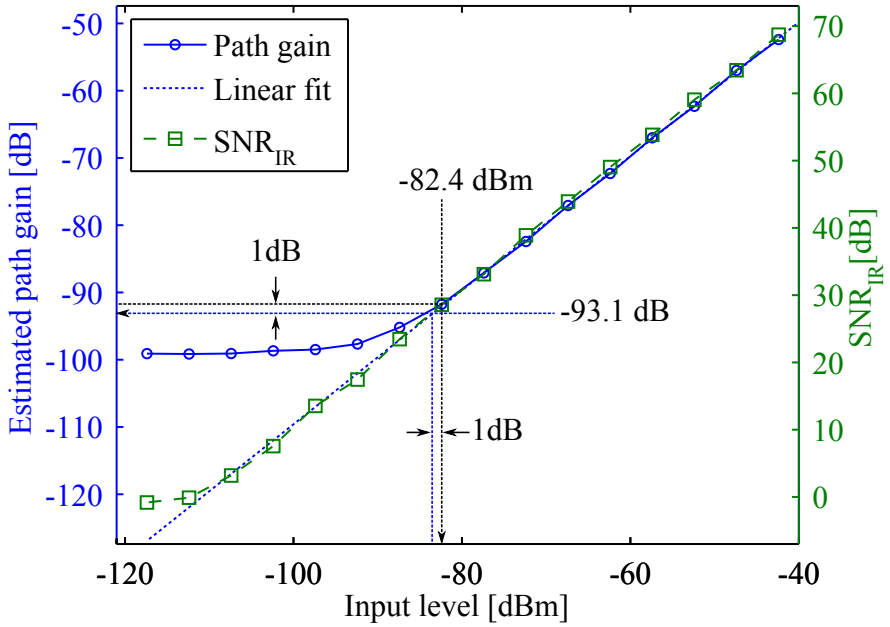

Figure 4.6 Variations of estimated path gain and SNR_{IR} in different input power level.

the right in Fig. 4.6 is SNR_{IR} which is defined as the power level difference between the peak and noise floor in estimated IR.

It was observed that the path gain could not be correctly estimated at the input power level below −82.4 dBm. Rx input level below 1 dB from this reference point was selected as the Rx sensitivity level, which corresponds to −93.1 dB insertion loss. The SNR_{IR} was 27.4 dB at sensitivity level. Therefore by including antenna gains of 19 dB and required SNR of 5.9 dB, total propagation loss of 106.2 dB can be allowed which corresponds to the measurement range of about 450 m in free-space. It was confirmed that the actual level of propagation loss allowed in the developed system well agreed with the design specification, and resulting dynamic performance is reasonable for the evaluation of micro cellular scenarios at 11 GHz [54].

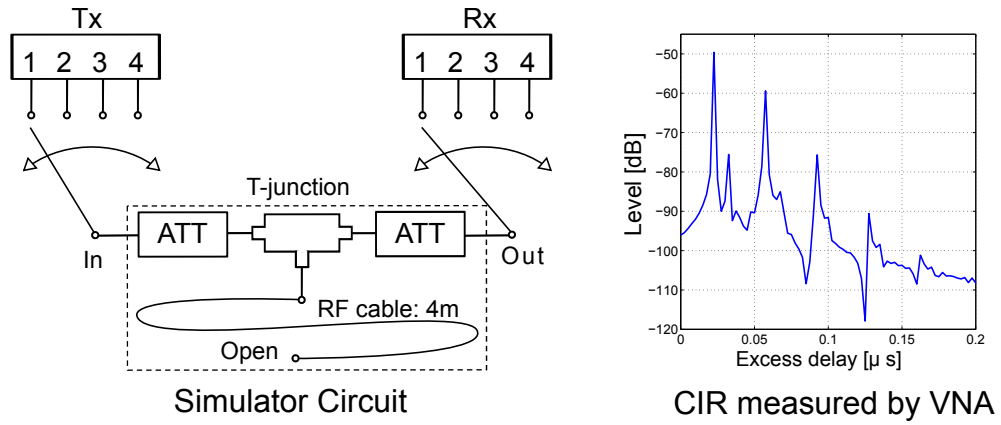

Figure 4.7 Blockdiagram of channel simulator circuit.

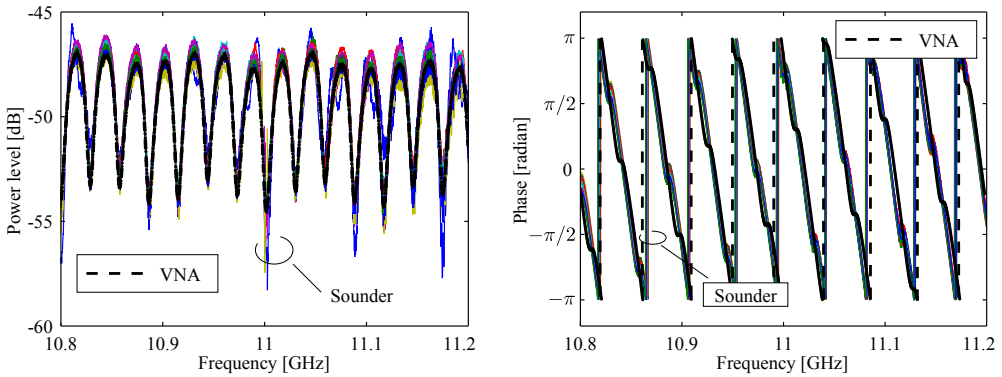

(a) Power level of transfer function. (b) Phase of transfer function.

Figure 4.8 Comparison with VNA in the test circuit measurements.

4.4 Test Circuit Measurement

To check overall system performance after the IQI compensation and back-to-back calibration, TFs measured by the developed sounder and a vector network analyzer (VNA) were compared. The internal LOs were used both at Tx and Rx to evaluate the influence of relatively large system PN identified in previous section. A channel simulator circuit was developed as shown in Fig. 4.7 to generate a reproducible channel in the repetitive measurements by the sounder and the VNA. The circuit is composed of a 4 m RF cable which was connected to a T-junction. The channel property can be kept

constant by fixing the shape of the RF cable. The channel response of the simulator circuit was measured in advance by the VNA as a reference. Fig. 4.8 shows the comparisons of measured TFs in terms of power level (Fig. 4.8(a)) and phase (Fig. 4.8(b)). Good agreement between measured TFs by the developed sounder and the VNA is obvious. Particularly, the influence of the system PN fluctuations within a frame length were not identified as shown by the agreement in the phase comparison. The results verified the performance of the developed sounder including the effects of several calibration techniques and other system imperfections.

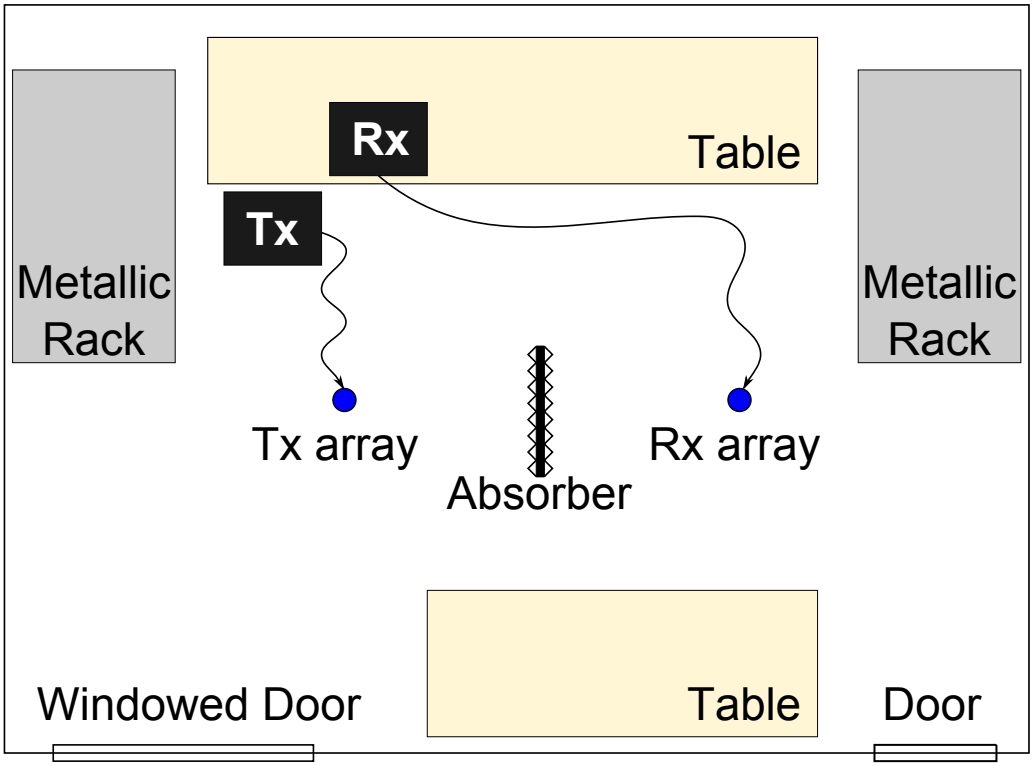

Figure 4.9 Layout of the indoor propagation test.

4.4.1 Indoor Propagation Measurement

Propagation measurement is conducted at experiment room in Tokyo Institute of Technology. Fig. 4.9 shows the layout of the measurement site. The

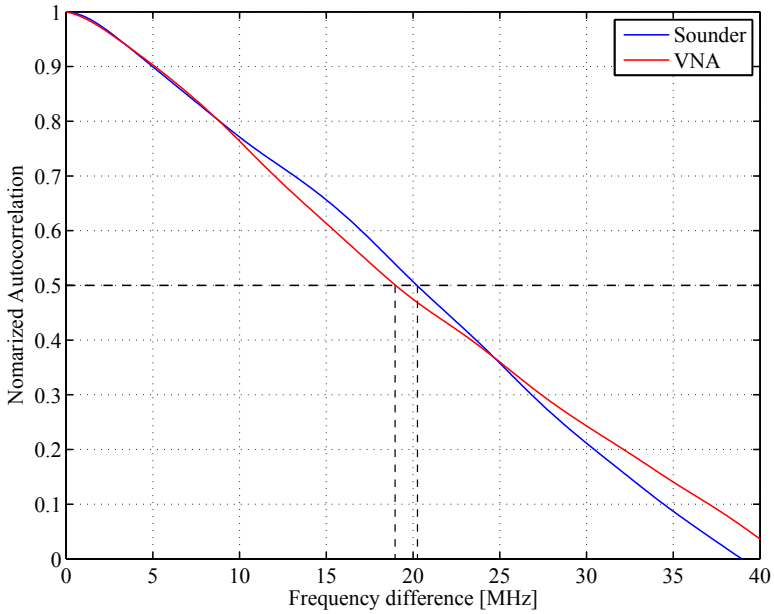

Figure 4.10 Comparison of frequency autocorrelation (normalized).

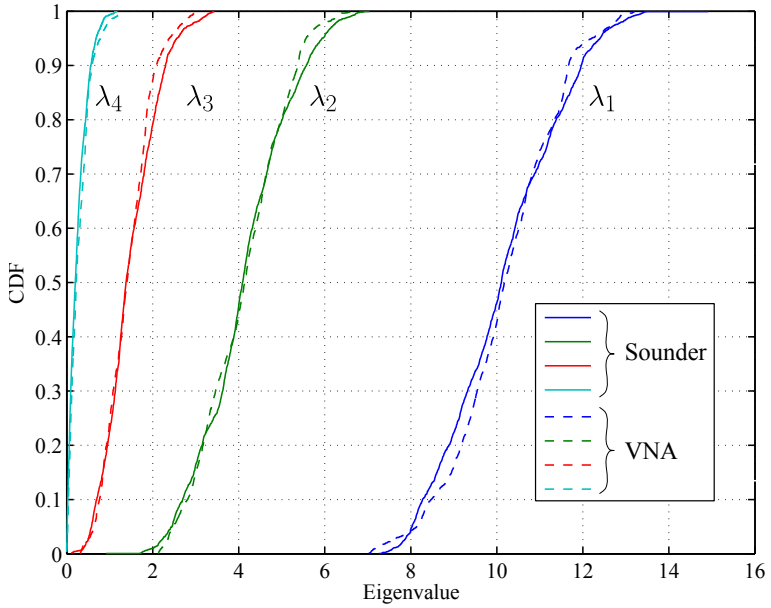

Figure 4.11 Comparison of eigenvalue CDF calculated for the 2048 subcarriers within single snapshot.

room is furnished with several tables and metallic racks. Radio wave absorber is placed between the Tx and Rx arrays to avoid clear LoS and saturation at

receiver system. The distance between Tx and Rx is set to 4 m. The VNA is used to obtain the reference data fixing the layout of the measurement layout. The channel stationarity is confirmed by taking comparing the 10 snapshots of 4×4 MIMO channel matrix using VNA.

Fig. 4.10 shows the normalized frequency autocorrelation function by sounder and VNA. The results shown are obtained by averaging all the elements of channel matrix. Measured frequency autocorrelation using developed sounder is well fitted with the results by VNA. The coherence bandwidth is computed as 20.2 MHz and 19.1 MHz from the results by sounder and VNA, respectively. The results of eigenvalue distributions are shown in Fig. 4.11. Distribution of all the eigenvalues could be well estimated by using channel sounder.

4.5 Summary

In this chapter, performance of the developed system including the proposed IQI compensation techniques and back-to-back calibration method were examined. For each of the hardware components, measurement for the influence of separated frequency references at Tx and Rx systems, characteristics of the two types of local oscillators were conducted. Also the receiver sensitivity which determines the applicable measurement range is carefully confirmed. It was observed that the performance of the hardware components were well within the level expected in design , although the system phase noise variation was relatively larger that result in the phase variation within sounding frame when internal normal-precision local oscillator was used.

The total performance of the developed system was also compared with commercial vector network analyzer (VNA) by two types of measurements: 1) direct-connection measurement using simulator circuit, 2) over-the air test in indoor environment to confirm the performance when measurement antennas were included. In both of the measurements, the results obtained by developed sounder showed the good agreement with the results from VNA.

Through the examinations presented in this chapter, the performance of the developed channel sounder is verified in the laboratory environment. The results from more realistic measurement is presented in Chapter 5.

Chapter 5

Measurement Campaign

5.1 Intdocution

This chapter presents the results from channel sounding in an indoor hall environment, that demonstrate the capability of the developed channel sounder in the multi-link channel characterization. Two measurements of *1)* directional measurements in terms of three Rx positions and *2)* simultaneous measurement of the three links were conducted sequentially. Since the Tx and Rx antennas were located at the same positions in both of the measurements and also the environment was maintained static during whole the measurement duration, two results can be comparable. That is to say, we can observe the angle-delay power spectrum for each link as well as the multi-link MIMO channel property, which can provide insightful information of the site-specific propagation mechanism. In the following sections, setup of the measurement is briefly explained in Sec. 5.2. To evaluate the performance of the developed channel sounder, measurement results are compared with the results from computer simulation by means of ray-tracing (sub-section 5.3.2). In sub-section 5.3.3, analysis on the inter-relation between inter-link correlation and the propagation mechanisms is shown.

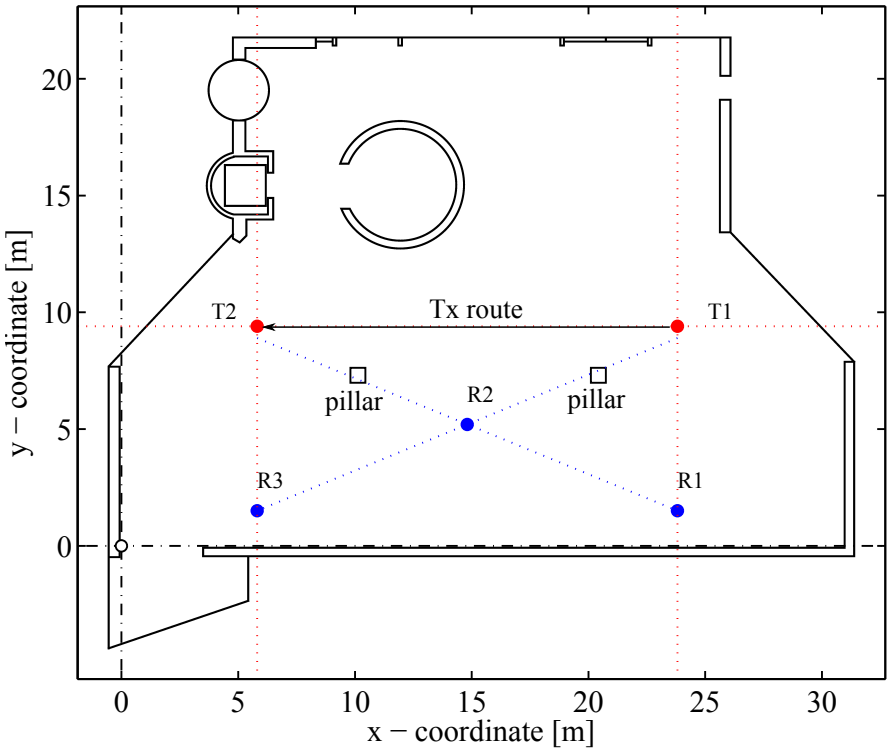

Figure 5.1 Floor plan of the indoor hall environment and layout of the measurement.

5.2 Measurement Setup

5.2.1 Overview of the measurement setup

Fig. 5.1 shows the floor plan of the indoor hall and layout of the measurements. The Tx was moved along the route from T1 to T2, and three Rxs were placed at R1, R2 and R3. Panoramic photos taken at each Rx position are shown in Fig. 5.2. All the three links share the line-of-sight (LoS) to most of the Tx positions except for the shadowing regions by two pillars. High-level diagrams of the measurement setup are shown in Fig. 5.3 and Fig. 5.4. A 10 MHz reference signal was shared among all the casings. The choice of LOs were based on the proposed synchronization setups shown in Fig. 2.2, i.e. external LOs for directional measurements, and internal LOs for *2)* three links simultaneous measurement.

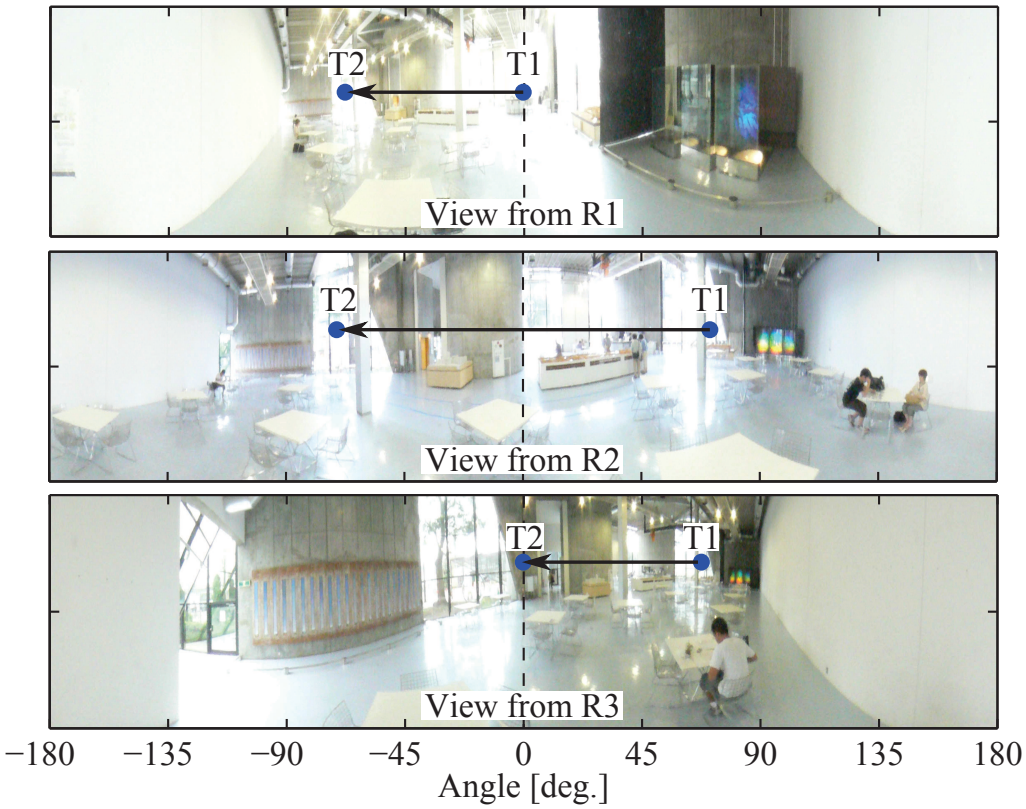

Figure 5.2 Photos taken at Rx positions R1, R2 and R3. (Blue dots indicate the Tx positions of T1 and T2.)

1. Single-link measurement
    - 10 MHz reference signal: shared by all the measurement system
    - 11 GHz LO signal: high-precision LO are used both at Tx and Rx
2. Multi-link measurement
    - 10 MHz reference signal: shared by all the measurement system
    - 11 GHz LO signal:
        - Tx side: High-precision external LO
        - Rx side: Normal-precision internal LO at each of Rx

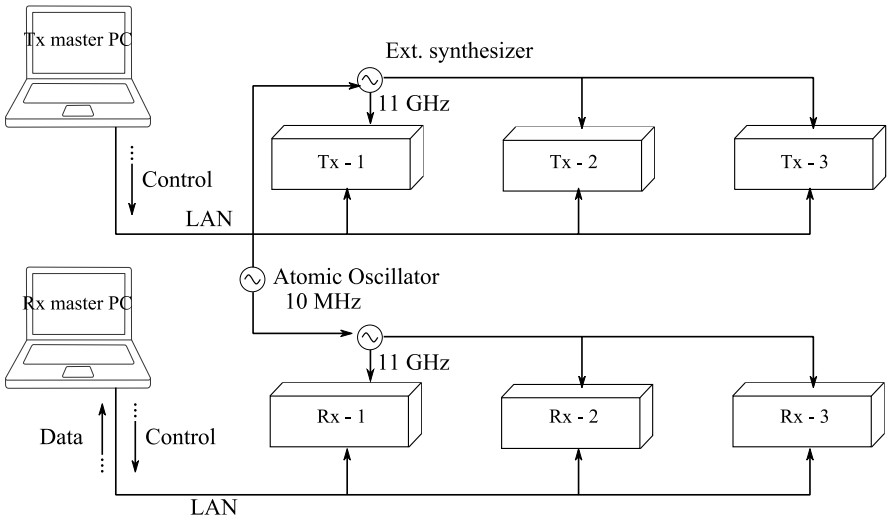

Figure 5.3 High-level diagram of the single-link measurement (external high-precision LO were used both at Tx and Rx).

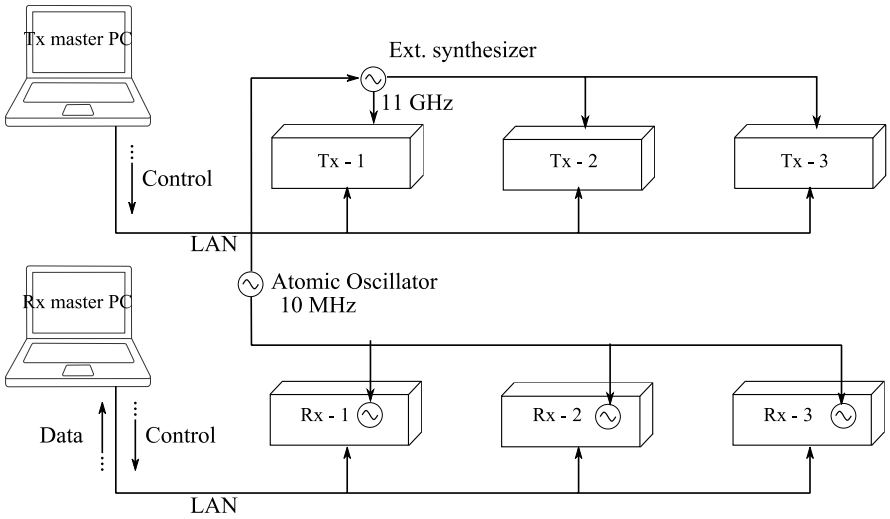

Figure 5.4 High-level diagram of the multi-link measurement. (external high-precision Lo was used at Tx, but at Rx side, internal normal-precision LOs were used to enable spatial separation of Rxs.)

5.2.2 Antenna orientation

In the single-link setup, 12-elements UCA were used both at Tx and Rx to enable double-directional angular estimation. In the multi-link setup, MU-MIMO down-link scenario was considered where the number of antenna elements were set to $N_{\text{tx}} = 6$, $N_{\text{rx}} = 2$ at each of three Rxs, where vertical polarized sleeve antennas with omni-directional directivity were used. Various antenna orientation were evaluated at Tx side as shown in Fig. 5.5 and Fig. 5.6 to know the realistic MIMO channel property and its antenna dependence. Antenna orientation at Rx side was kept same for all the multi-link measurements as shown in Fig. 5.7.

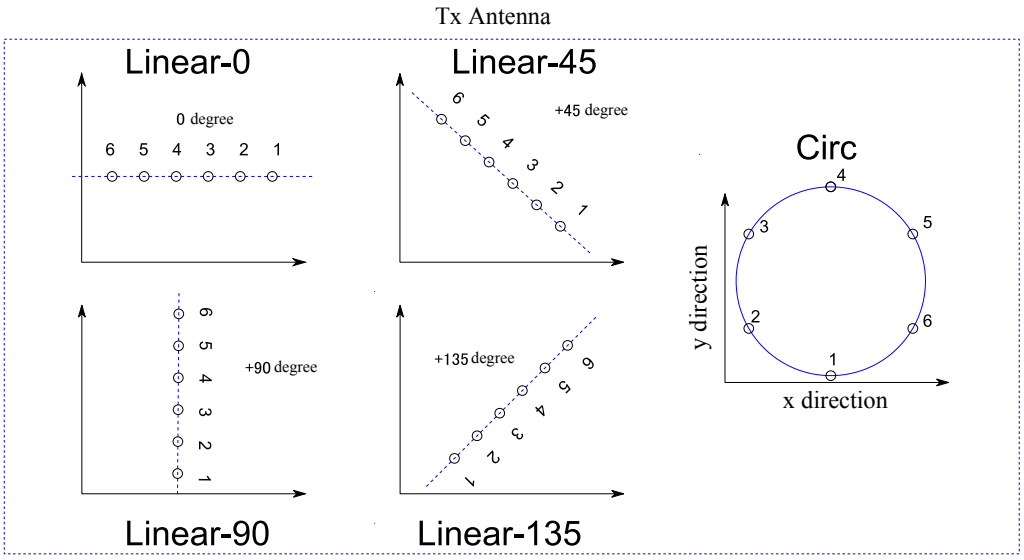

Figure 5.5 Antenna orientation at Tx for multi-link measurement.

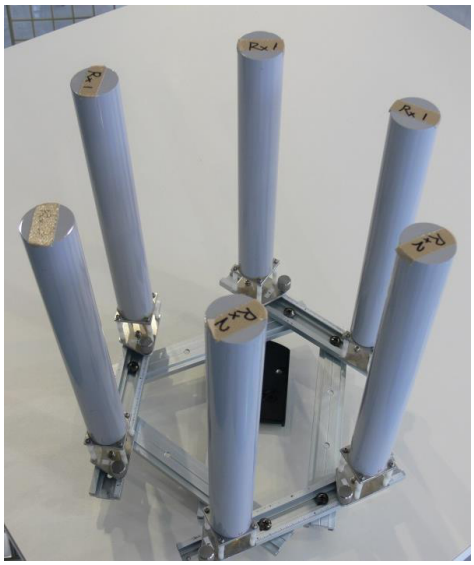

Figure 5.6 Photo of the antenna orientation at Tx for multi-link measurement (6-elements configuration).

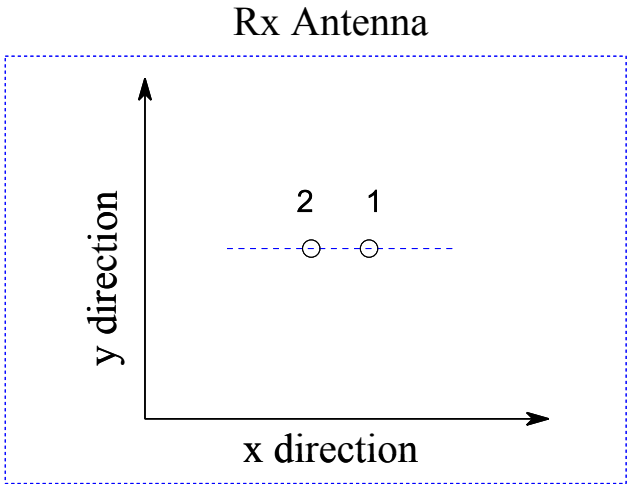

Figure 5.7 Antenna orientation at Rx for multi-link measurement.

5.3 Results

In this section, measurement results from indoor hall environment were analyzed. First in sub-section 5.3.1, results of fundamental channel properties are shown including evaluation of the influence of measurement antenna. Sub-section 5.3.2 shows the comparison of measurement results and simulated results based on commercial ray-tracing simulator [55]. The comparison aimed at verifying the fundamental performance of the developed channel sounder and applied calibration method. Finally in sub-section 5.3.3, observed inter-link correlation is discussed based on the propagation mechanism obtained by single-link measurement.

5.3.1 Fundamental analysis

It should be noted that both of the measurement results by single-link directional and multi-link simultaneous measurements include the influence of measurement antenna. Therefore in precise sense, conducted two measurements can not be compared each other without applying antenna de-embedding processing. In general, antenna de-embedding can be achieved by applying super-resolution parameter estimation such as SAGE [56], however, it is not considered in this study. Also in the following, data analyses are all based on the measured channel for vertical polarization, and 6-elements circular array (as shown in Fig. 5.6) in multi-link setup. To check the influence of measurement antenna, delay power spectrum of single-link and multi-link measurements are compared as shown in Fig. 5.8. The results in left column of Fig. 5.8 (i.e. figures (a), (c) and (e)) are the delay power spectrum simultaneously measured in multi-link measurement. On the other hand, the results in right column (i.e. figures (b), (d) and (f)) were sequentially measured one-by-one in single-link measurements by changing the positions of Rx antennas. The results show that the line-of-sight (LoS) components and other primal clusters are well agreed in two measurement setups. Moreover the clusters traveled relatively long path lengths are also observed in both of the setups. Accordingly, although the single-link setup were not measured

simultaneously and influences of the measurement antennas were included, results from two setups could be considered as comparative under the static channel environments.

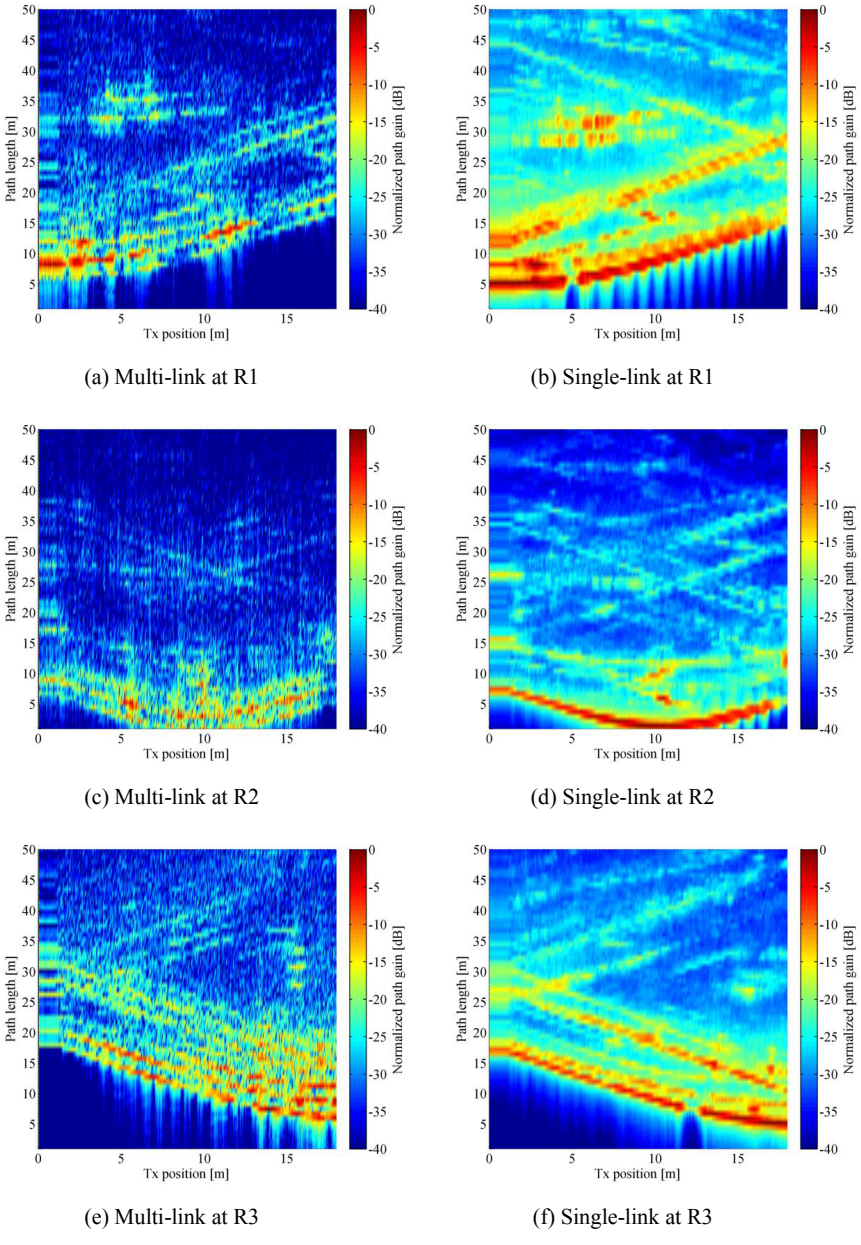

(a) Multi-link at R1

(b) Single-link at R1

(c) Multi-link at R2

(d) Single-link at R2

(e) Multi-link at R3

(f) Single-link at R3

(Delay is converted into paht length [m])

Figure 5.8 Delay power spectrum obtained by multi-link (left column) and single-link (right column) setups.

5.3.2 Comparison with the ray-tracing simulation

In this sub-section, measurement results are compared with ray-tracing simulation based on detailed building model obtained by 3D laser scanner. Although the channel sounder measurement provides most realistic channel properties, the estimated propagation mechanism is heavily dependent on the channel sounder performance. For example in the developed channel sounder in this study, the delay resolution is 2.5 ns (75 cm in path length) and the angular resolution is limited to about 23 °. Therefore without applying super-resolution parameter estimation, detailed analysis of propagation mechanism is challenging in angular dimension. In this regard, use of ray-tracing simulation to support and verify the channel sounder measurement is very useful.

5.3.2.1 Process of 3D ray-tracing simulation

1. Production of building model
   3D point cloud data sets are first converted into CAD-based building model. Fig. 5.9 shows the process of building model generation from point clouds data sets to simplified 3D model suited for ray-tracing simulation. In the processing of 3D simplified model generation (from (b) to (c)), relatively small objects included in the 3D CAD model in (b) were removed and build as surface model. Also the building materials are expressed by concrete and glass which have different reflection characteristics.

2. Execution of the ray-tracing simulation
   For the execution of the ray-tracing simulation, commercial ray-tracer of Raplab [55] was selected. For the purpose of simplification, number of reflection is set to 2 times and only single diffraction is calculated. Also the reflection from roof is not included since the roof height can be considered as enough high. For the antenna model, omni-directional dipole antenna is assumed both at Tx and Rx.

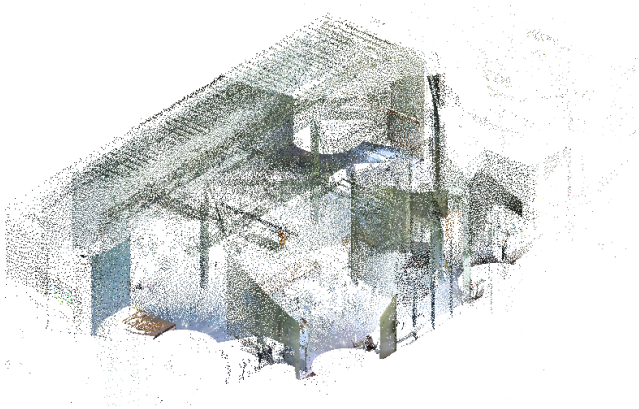

(a) Point clound data measured by 3D scanner.

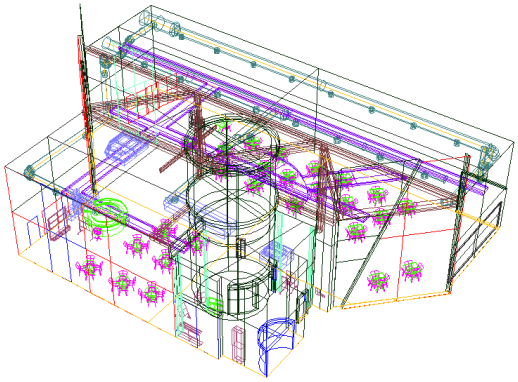

(b) Detailed CAD building model obtained from point cloud data.

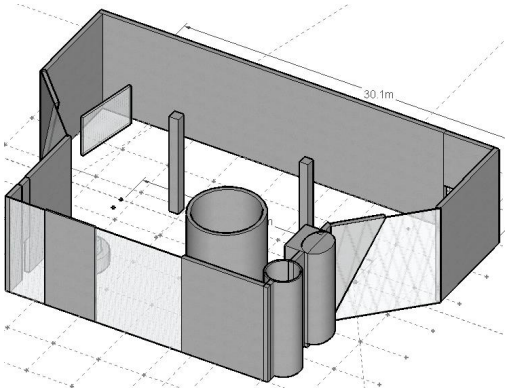

(c) Simplified 3D building model for ray-tracing simulation.

Figure 5.9 Process of 3D building model generation. (a): 3D point cloud data sets, (b): 3D CAD model obtained from point clouds and (c) simplified 3D surface model used in ray-tracing simulation.

3. Simulation result example
   As a result of ray-tracing simulation, detailed channel parameters such as path loss, angle of departure, angle of arrival and propagation path (reflection and diffraction points) were obtained. Fig. 5.10 shows the example results in 2D and 3D views.

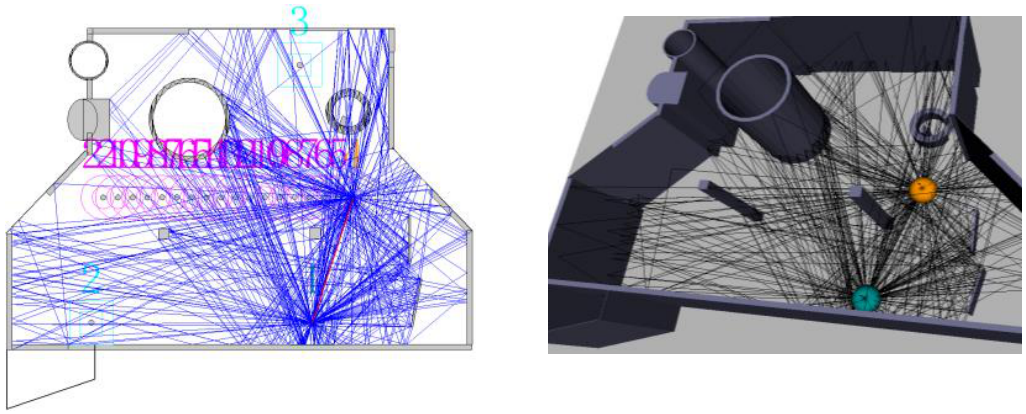

(a) 2D view (b) 3D view

Figure 5.10 Example results of ray-tracing simulation in 2D and 3D views..

5.3.2.2 Reconstruction of system dependent channel response from the ray-tracing simulation

In the ray-tracing simulation, propagation channel is expressed as geometrical optics based on high-frequency approximation. Therefore, resolution of the obtained channel parameters have infinite delay and angular resolution, are the comparison with measurement results becomes difficult. In the following processing, system dependent (band-limited) channel responses are reconstructed. The reconstruction is done assuming following signal model which consists of l propagation paths.

$$\mathbf{H}(f) = G_{\mathrm{R}}(f) \sum_{l=1}^{L} \left(b_f(\tau_l) \cdot \mathbf{B}_{\mathrm{R}}(\phi_{\mathrm{R},l}, \theta_{\mathrm{R},l}) \cdot \begin{bmatrix} \gamma_{\mathrm{HH},l} & \gamma_{\mathrm{VH},l} \\ \gamma_{\mathrm{HV},l} & \gamma_{\mathrm{VV},l} \end{bmatrix} \cdot \mathbf{B}_{\mathrm{T}}^{T}(\phi_{\mathrm{T},l}, \theta_{\mathrm{T},l}) \cdot \right) G_{\mathrm{T}}(f) \qquad (5.1)$$

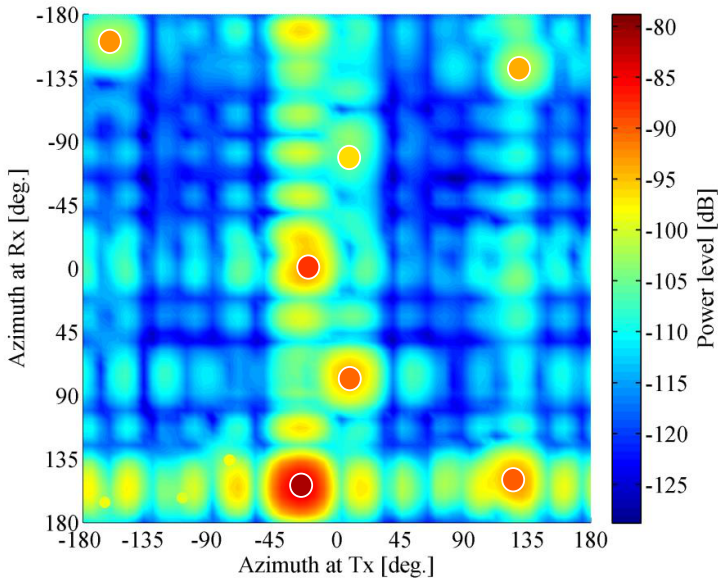

Figure 5.11 Comparison of double-directional angular power spectrum: ray-tracing outputs and reconstructed channel response.(The ray-tracing outputs paths are indicated by the colored dots.)

where, $G_{\mathrm{R}(f)}$ and $G_{\mathrm{T}(f)}$ are the TFs of Rx and Tx respectively. $\mathbf{B}_{\mathrm{R}}(\phi_{\mathrm{R},l}, \theta_{\mathrm{R},l})$ and $\mathbf{B}_{\mathrm{T}}(\phi_{\mathrm{T},l}, \theta_{\mathrm{T},l})$ are the radiation patterns of Rx and Tx antennas respectively. $b_f(\tau_l)$ is the phase rotation due to propagation delay, γ is the complex path weight which corresponds to complex amplitude components of each of the polarization pairs. In the channel response reconstruction, radiation pattern of the 12-elements UCA measured in an anechoic chamber was used, and outputs from ray-tracing simulation were used for other parameters (delay, path loss, angle-of-departure and arrival). Fig. 5.11 shows the double-directional angular power spectrum obtained from reconstructed channel response (beamforming is applied). Well agreement between ray-tracing outputs and reconstructed angler power spectrum shows the validity of the applied reconstruction processing.

5.3.2.3 Comparison and discussion

Fig, 5.12 shows the variations of delay, angle-of-departure and angle-of-arrival power spectrum for measured and simulated channels. The results in the left column of Fig. 5.12 are obtained from reconstructed channel response using ray-tracing outputs. The results in the right column are obtained from measured channel utilizing the developed channel sounder. In all the dimensions, simulated and measured results are agreed well. However at the specific Tx antenna positions, some propagation paths were not observed in simulated channel compared with measured one as follows.

- Fig. 5.12 (b): Path length $\approx 35 \sim 40$ m
- Fig. 5.12 (d): Angle-of-departure $\approx 100^\circ$ (Tx at 3 m position)
- Fig. 5.12 (f): Angle-of-arrival $\approx 0^\circ$ (Tx at 4 m position)

The reason for the above differences can not be exactly explained by either of lack of building model accuracy or measurement reliability. For more detailed analysis, ray-tracing simulation should be conducted by using more detailed building model so to consider the influence of the neglected small objects.

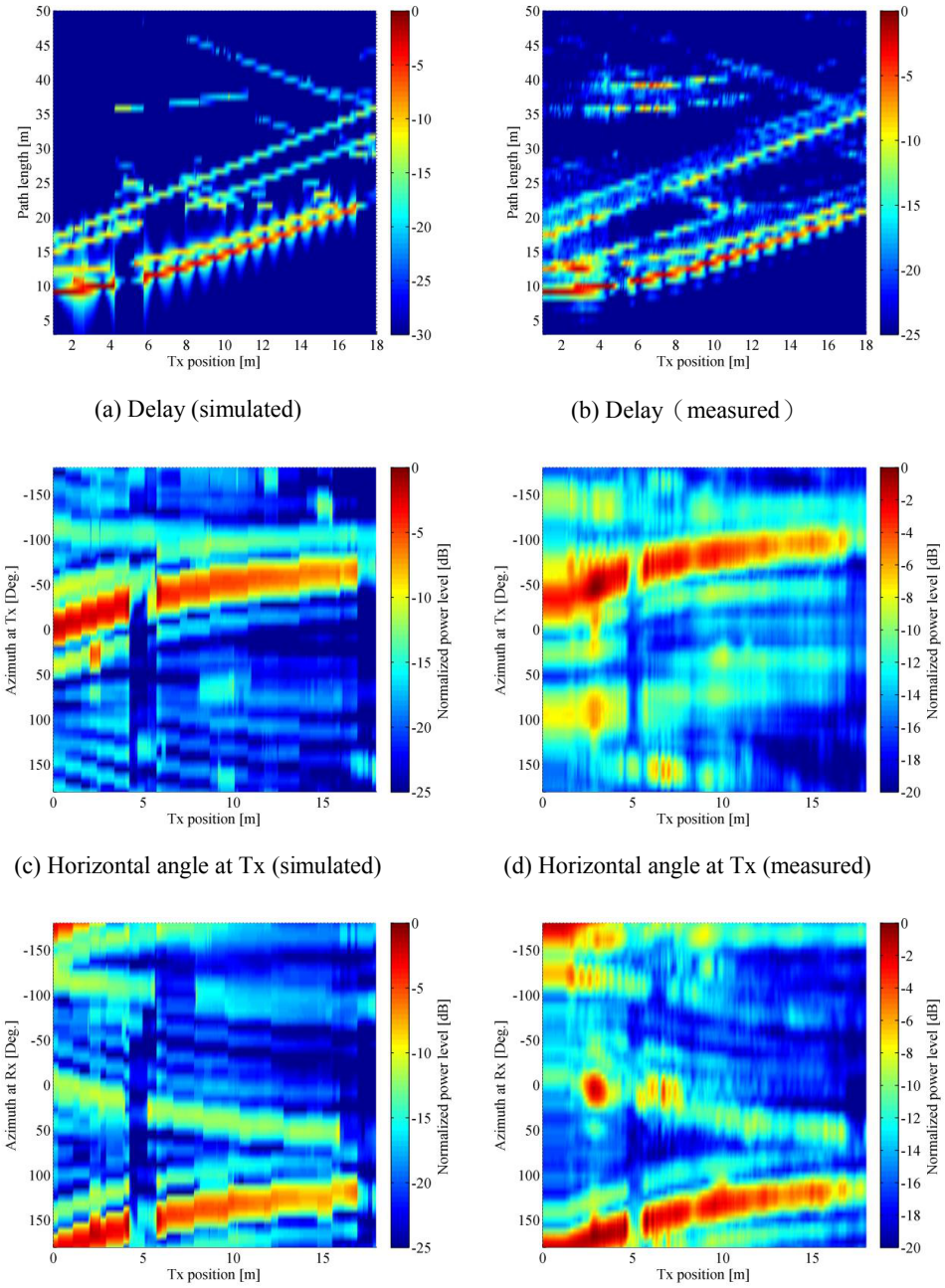

(a) Delay (simulated)

(b) Delay（measured）

(c) Horizontal angle at Tx (simulated)

(d) Horizontal angle at Tx (measured)

(e) Horizontal angle at Rx (simulated)

(f) Horizontal angle at Rx (measured)

Figure 5.12 Variations of power spectrum in delay, angle-of-departure and angle-of-arrival domains for measured and simulated channels.

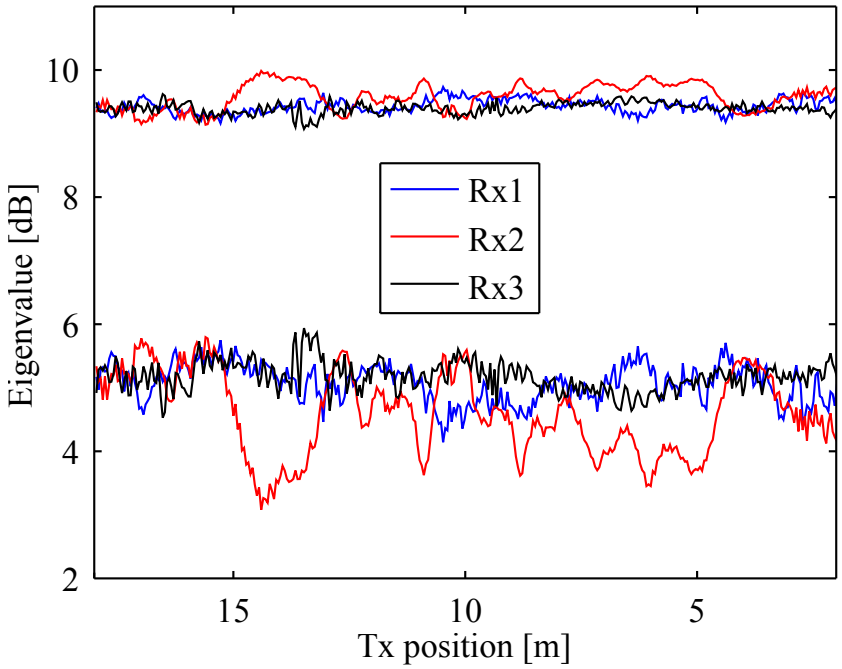

Figure 5.13 Eigenvalue variations measured in simultaneous measurement of three links.

5.3.3 Analysis of propagation mechanisms and inter-link correlation

From the simultaneous measurement of three links, eigenvalues of 2×6 MIMO channel matrix were obtained for each of the links as shown in Fig. 5.13. The three MIMO channel matrices were individually normalized as

$$\hat{\mathbf{H}}_i(s) = \frac{\mathbf{H}_i(s)}{\sqrt{P_i}}, \tag{5.2}$$

where

$$P_i = \frac{1}{N_\mathrm{s} N_\mathrm{r} N_\mathrm{t}} \sum_{s=1}^{N_\mathrm{s}} \|\mathbf{H}_i(s)\|_\mathrm{F}^2 \,. \tag{5.3}$$

In the equations, s is the snapshot index corresponding to the Tx positions, $\mathbf{H}_i(s)$ is the channel matrix of the i-th link, and $\|\bullet\|_\mathrm{F}$ returns the Frobenius

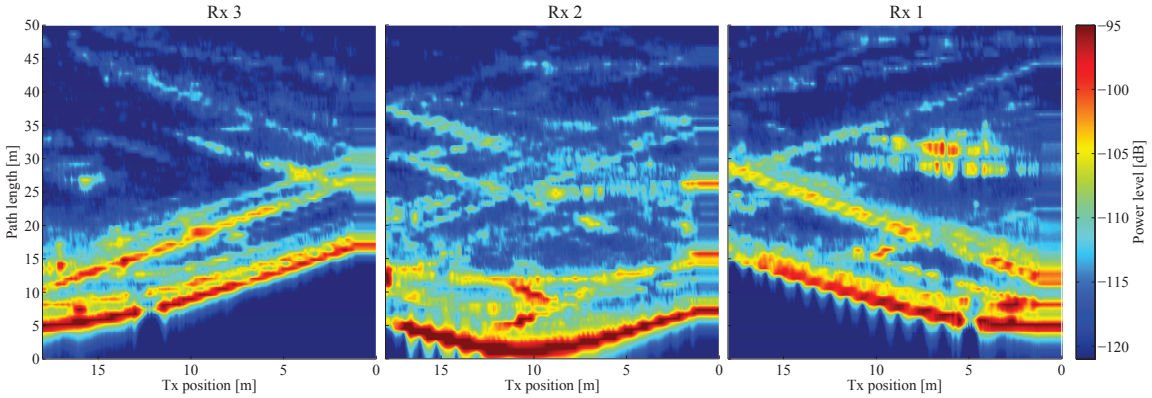

Figure 5.14 Variations of delay power spectrum at R1, R2 and R3 estimated in directional measurement setup.

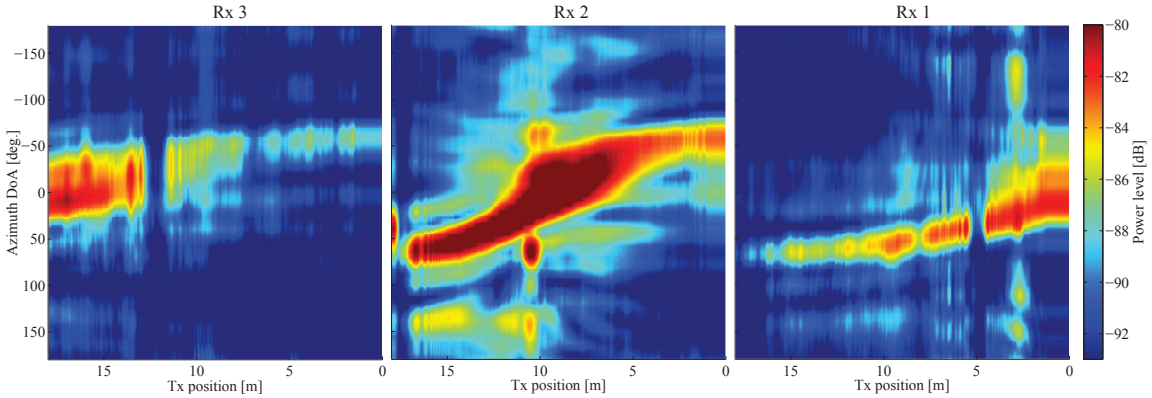

Figure 5.15 Variations of DoA power spectrum at R1, R2 and R3 estimated in directional measurement setup.

norm. In Fig. 5.13, the eigenvalues did not change significantly except at Rx2 when Tx was moving around Tx positions 4 m and 14 m.

To obtain insights regarding directional propagation mechanism, Fig. 5.14 and Fig. 5.15 show the estimated power spectrum variations in terms of path length and direction-of-arrival (DoA) domains, respectively, which were estimated from the directional measurements. The DoA power spectrum was obtained by means of Bartlett beamformer [57] utilizing the calibrated antenna radiation patterns of UCA. Strong LoS components and shadowing effects by pillars were clearly illustrated. The observed eigenvalue fluctuations at Rx2 can be explained from the identified propagation mechanism

since LoS components were always significant at Rx2 even around the shadowing region by pillars, while the level of strongest non-LoS components were decreased around the shadowing region. This phenomenon did not happen at other Rx positions.

5.4 Summary

The measurements were aimed at examination of sounder capability in a realistic measurement condition. A simultaneous multi-link measurement provided the MIMO channel condition at three links simultaneously influenced by the shadowing effect. Directional spectrum could be obtained from repetition of single-link measurement with same layout as mutl-link setup. Comparative analysis of the results from two measurements enabled the physical interpretation of multi-link MIMO channel performance, hence demonstrated the capability of the developed scalable channel sounder.

Chapter 6

Conclusions

6.1 Concluding Remarks

In this dissertation, a 24×24 MIMO channel sounder that has been developed based on a scalable fully-parallel MIMO architecture was proposed so that it can be flexibly configured with 3 Tx and Rx casings, each of which has 8 antennas. This flexibility allows the measurement for various purposes including double-directional channel modeling and investigation of multi-link MIMO communication systems, which can provide insightful information for the evaluation of multi-link cooperative MIMO communication systems.

Several calibration techniques were implemented to solve the practical issues related to the multi-link operation and the fully-parallel architecture. The resulting system performance was validated through various evaluation experiments regarding the influences of separated frequency references, system phase noise and dynamic performance. Finally, the results from directional and multi-link channel measurements in an indoor environment demonstrated the capability of the developed system.

6.2 Contributions

The contributions that have been developed in this thesis are listed as follows.

- development of measurement system for double-directional and multi-link channel investigation
- identification of practical issues when extending generic MIMO testbed into directional-multi-link channel sounder
- development of simple calibration techniques appropriate for field operation
- clarification of synchronization requirements at 11 GHz frequency band

6.3 Future Prospects

There are several prospect related in this research that may be considered in the future studies. So the suggested topics are listed in the following.

1. Study on alternative synchronization methods
   Cesium frequency standards are utilized in this thesis as reference signals for the complete separation of Tx and Rx systems, despite its drawback in cost and spatial size. This was due to the significant long-term phase drift at 11 GHz. However, if the short-term stability of the system phase noise is dominated by the performance of local oscillator, Rubidium oscillator may be utilized by keeping the long-term stability by global positioning system (GPS).
2. Study on frequency-dependent IQ imbalance compensation
   Since the developed IQ compensation techniques in this thesis assumed the frequency-independent hardware characteristics. This assumption may not be satisfied in the system that has broader bandwidth such as ultra-wide–band (UWB) communication systems.

3. Study on non-linear distortion at RF analog front-end
   Through the performance evaluation of the RF analog-front-end at transmitter side, relatively strong 2nd harmonic distortion was observed, and that component could not be compensated by the digital pre-distortion technique utilized in this study. The study on the mechanism of the observed non-linear distortion and development of the compensation technique is interesting to be considered, since that is also beneficial for the development of MIMO transmission system.

4. Implementation of real-time transmission signal processing
   Since the developed channel sounder shares its architecture with generic MIMO transmission systems, implementation of real-time transmission processing and simultaneous field testing of transmission performance and propagation channel analysis is possible. It will provides insightful information on the site-specific evaluation of MIMO system from both the aspects of transmission performance and channel condition in that instant.

References

[1] S. Cherry, "Edholm's Law of Bandwidth," *IEEE Spectrum*, vol. 41, no. 7, pp. 51–52, Jul 2004.

[2] J. Winters, "On the capacity of radio communication systems with diversity in a rayleigh fading environment," *IEEE J. Sel. Areas Commun.*, vol. 5, no. 5, pp. 871 – 878, Jun. 1987.

[3] G. J. Foschini and M. J. Gans, "On Limits of Wireless Communications in a Fading Environment when Using Multiple Antennas," *Wireless Personal Commun.*, vol. 6, pp. 311–335, 1998.

[4] E. Telatar, "Capacity of multi-antenna gaussian channels," *European transactions on telecommunications*, vol. 10, no. 6, pp. 585–595, 1999.

[5] ITU-R M.2078, "Estimated spectrum bandwidth requirements for the future development of IMT-2000 and IMT-Advanced," 2006.

[6] ITU-R M.2134, "Requirements related to technical performance for IMT-Advanced radio interface (s)," 2008.

[7] L. Liu, R. Chen, and S. Geirhofer, "Downlink MIMO in LTE-advanced: SU-MIMO vs. MU-MIMO," *IEEE Commun. Mag.*, pp. 140–147, Feb. 2012.

[8] D. Lee, H. Seo, and B. Clerckx, "Coordinated multipoint transmission and reception in LTE-advanced: deployment scenarios and operational challenges," *IEEE Commun. Mag.*, pp. 148–155, Feb. 2012.

[9] 3GPP TR 36.912, "Feasibility study for Further Advancements for E-UTRA (LTE-Advanced)," Oct. 2012.

[10] C. Wang, X. Hong, X. Ge, X. Cheng, G. Zhang, and J. Thompson, "Cooperative MIMO channel models: a survey," *IEEE Commun. Mag.*, vol. 48, no. 2, pp. 80 –87, Feb. 2010.

[11] C. Oestges, "Multi-link propagation modeling for beyond next generation wireless," in *Proc. Loughborough Antennas and Propagation Conf. (LAPC)*, Nov. 2011.

[12] V. Kolmonen, K. Haneda, T. Hult, J. Poutanen, F. Tufvesson, and P. Vainikainen, "Measurement-Based Evaluation of Interlink Correlation for Indoor Multiuser MIMO Channels," *IEEE Antennas and Wireless Propagation Letters*, vol. 9, pp. 311–314, 2010.

[13] J. Poutanen, K. Haneda, V.-m. Kolmonen, J. Salmi, and P. Vainikainen, "Analysis of Correlated Shadow Fading in Dual-Link," *IEEE Antennas and Wireless Propagation Letters*, vol. 8, pp. 1190–1193, 2009.

[14] J. Poutanen, K. Haneda, J. Salmi, V. Kolmonen, F. Tufvesson, T. Hult, and P. Vainikainen, "Significance of common scatterers in multi-link indoor radio wave propagation," in *Proceedings of the Fourth European Conference on Antennas and Propagation (EuCAP), 2010*, 2010.

[15] V. Kolmonen, P. Almers, J. Salmi, J. Koivunen, K. Haneda, A. Richter, F. Tufvesson, A. Molisch, and P. Vainikainen, "A dynamic dual-link wideband MIMO channel sounder for 5.3 GHz," *IEEE Trans. Instrum. Meas.*, vol. 59, no. 4, pp. 873 –883, Apr. 2010.

[16] "MEDAV RUSK Channel Sounder." [Online]. Available: http://www.channelsounder.de/

[17] K. Mizutani, K. Sakaguchi, J. Takada, and K. Araki, "Development of MIMO-SDR Platform and Its Application to Real-Time Channel Measurements," *IEICE Trans. Commun.*, vol. E89-B, no. 12, pp. 3197 – 3207, Dec. 2006.

[18] N. Costa and S. Haykin, "A Novel Wideband MIMO Channel Model and the Wideband MIMO Software Defined Radio," in *Proc. Int. Conf. on Wireless Commun., Networking and Mobile Computing, 2006 (WiCOM 2006)*, Sep. 2006.

[19] J. Gutiérrez, O. González, J. Pérez, D. Ramirez, L. Vielva, J. Ibáñez, and I. Santamaria, "Frequency-Domain Methodology for Measuring MIMO Channels Using a Generic Test Bed," *IEEE Trans. Instrum. Meas.*, vol. 60, no. 3, pp. 827–838, Mar. 2011.

[20] R. S. Thomä, M. Landmann, A. Richter, and U. Trautwein, "Multi-dimensional high-resolution channel sounding measurement," in *Smart antennas: state of the art*, T. Kaiser, Ed. Hindawi Pub Corp, 2005, ch. 13, pp. 241–270.

[21] J. Andersen, J. Nielsen, G. Pedersen, K. Olesen, P. Eggers, E. Sorensen, and S. Denno, "A 16 by 32 wideband multichannel sounder at 5 GHz for MIMO," in *Proc. IEEE Antennas and Propagation Soc. Int. Symp.*, Jun. 2004.

[22] V. Kolmonen, J. Kivinen, L. Vuokko, and P. Vainikainen, "5.3-GHz MIMO radio channel sounder," *IEEE Trans. Instrum. Meas.*, vol. 55, no. 4, pp. 1263 – 1269, Aug. 2006.

[23] R. Thomä, D. Hampicke, A. Richter, G. Sommerkorn, A. Schneider, U. Trautwein, and W. Wirnitzer, "Identification of time-variant directional mobile radio channels," *IEEE Trans. Instrum. Meas.*, vol. 49, no. 2, pp. 357 –364, Apr. 2000.

[24] D. Laurenson and P. Grant, "A review of radio channel sounding techniques," in *Proc. 14th European Signal Process. Conf.*, Florence, Italy, Sep. 2006.

[25] M. Steinbauer, A. Molisch, and E. Bonek, "The double-directional radio channel," *IEEE Antennas Propagat. Mag.*, vol. 43, no. 4, pp. 51 –63, Aug. 2001.

[26] U. Dótsch and J. Koppenborg, "Real-time Implementation and Trials of Advanced Receiver and Uplink CoMP Schemes," in *Coordinated Multi-Point in Mobile Communications* , P. Marsch and G. P. Fettweis, Eds. Cambridge University Press, 2011, ch. 13.1, pp. 313–319.

[27] R. Irmer, H. Droste, P. Marsch, M. Grieger, G. Fettweis, S. Brueck, H.-P. Mayer, L. Thiele, and V. Jungnickel, "Coordinated multipoint: Concepts, performance, and field trial results," *IEEE Commun. Mag.*, vol. 49, no. 2, pp. 102 –111, Feb. 2011.

[28] C. Mehlfü andhrer, S. Caban, and M. Rupp, "Measurement-Based Performance Evaluation of MIMO HSDPA," *IEEE Trans. Veh. Technol.*, vol. 59, no. 9, pp. 4354 –4367, Nov. 2010.

[29] M.-D. Kim, J. J. Park, H. K. Chung, and X. Yin, "Cross-correlation characteristics of multi-link channel based on channel measurements at 3.7GHz," in *Proc. 14th Int. Conf. on Advanced Commun. Technology (ICACT2012)*, Feb. 2012, pp. 351 –355.

[30] K. Nishimori, R. Kudo, N. Honma, Y. Takatori, and M. Mizoguchi, "16× 16 Multiuser MIMO Testbed Employing Simple Adaptive Modulation Scheme," in *Proc. IEEE 69th Vehicular Technology Conf. (VTC Spring 2009)*, Apr. 2009.

[31] C. Oestges and N. Czink, "Empirical investigation of multi-link separation for indoor MIMO channels," in *Proc. IEEE 22nd Int. Symp. on Personal Indoor and Mobile Radio Communications (PIMRC 2011)*, Sep. 2011.

[32] N. Czink, B. Bandemer, C. Oestges, T. Zemen, and A. Paulraj, "Analytical Multi-User MIMO Channel Modeling: Subspace Alignment Matters," *IEEE Trans. Wireless Commun.*, vol. 11, no. 1, pp. 367 –377, Jan. 2012.

[33] F. Kaltenberger, L. Cardoso, M. Kountouris, R. Knopp, and D. Gesbert, "Real-time Multi-user MIMO Channel Sounding and Capacity Evaluations," no. 08, pp. 0–11, 2008.

[34] N. Czink, B. Bandemer, G. Vazquez-Vilar, L. Jalloul, C. Oestges, and A. Paulraj, "Spatial separation of multi-user MIMO channels," in *IEEE 20th International Symposium on Personal, Indoor and Mobile Radio Communications (PIMRC2009)*. IEEE, 2009, pp. 1059–1063.

[35] M. Narandxic, M. Kaske, S. Jackel, G. Sommerkorn, C. Schneider, and R. S.Thoma., " Variation of estimated large-scale MIMO channel properties between repeated measurements," in *COST2100 TD-10-11088, Aalborg*, Jun 2010.

[36] V. Jungnickel, A. Forck, S. Jaeckel, S. Wahls, L. Thiele, T. Haustein, W. Zirwas, H. Droste, and G. Kadel, *Realtime Implementation and Field Trials for Downlink CoMP*, ser. Coordinated Multi-Point in Mobile Communications. Cambridge University Press, 2012, ch. 13.3.

[37] M. Kim, J. Takada, and Y. Konishi, "A Novel Scalable MIMO Channel Sounding Technique and Measurement Accuracy Evaluation with Transceiver Impairments," *IEEE Trans. Instrum. Meas.*, vol. 61, no. 12, pp. 3185–3197, Dec. 2012.

[38] M. Kim, Y. Konishi, J. Takada, and B. Gao, "Automatic IQ imbalance compensation technique for quadrature modulator by single-tone testing," *IEICE Trans. Commun.*, vol. E95-B, no. 5, p. 18641868, May 2012.

[39] M. Landmann, "Limitations of Experimental Channel Characterisation," Ph.D. dissertation, Ilmenau University of Technology, 2007.

[40] "Rubidium oscillator, Stanford Research Systems." [Online]. Available: http://www.thinksrs.com/products/FS725.htm

[41] "Cesium frequency standard, Symmetricom." [Online]. Available: http://www.symmetricom.com/products/frequency-references/cesium-frequency-standard/5071A/

[42] "TD-SPP3000, Tokyo Electron Device Ltd." [Online]. Available: http://www.inrevium.jp/pm/image_signal/spp3000.html

[43] "Virtex-5 FPGA, Xilinx Inc." [Online]. Available: http://www.xilinx.com/onlinestore/silicon/online_store_v5.htm

[44] "DAC5682, Texas Instruments Inc." [Online]. Available: http://www.ti.com/product/dac5682z

[45] "ADS5400, Texas Instruments Inc." [Online]. Available: http://www.ti.com/product/ads5400

[46] "MC10EP195, ON Semiconductor." [Online]. Available: http://www.onsemi.com/PowerSolutions/product.do?id=MC10EP195

[47] S. Suyama, H. Fukuda, H. Suzuki, and K. Fukawa, "10 Gbps 8×8 MIMO-OFDM broadband experimental system for 11 GHz band super high bit-rate mobile communications," in *Proc. Inter. OFDM-Workshop 2012*, Aug. 2012.

[48] "CompactPCI standard, PICMG." [Online]. Available: http://www.picmg.com/v2internal/resourcepage2.cfm?id=4

[49] A. Abidi, "Direct-conversion radio transceivers for digital communications," *IEEE J. Solid-State Circuits*, vol. 30, no. 12, pp. 1399 –1410, Dec. 1995.

[50] H. Arslan and H. Mahmoud, "Error vector magnitude to SNR conversion for nondata-aided receivers," *IEEE Trans. Wireless Commun.*, vol. 8, no. 5, pp. 2694 –2704, May 2009.

[51] O. Mylläri, L. Anttila, and M. Valkama, "Digital Transmitter I/Q Imbalance Calibration: Real-time Prototype Implementation and Performance Measurement," in *Proc. EURSIPCO*, Aug. 2010, pp. 537–541.

[52] M. Kim, Y. Maruichi, and J. Takada, "Parametric Method of Frequency-dependent I/Q Imbalance Compensation for Wideband Quadrature Modulator," *IEEE Trans. Microwave Theory Tech.*, vol. 61, no. 1, Jan 2013.

[53] M. Lin and I. Wassell, "Impact of Channel Sounder Frequency Offsets on the Estimation of Channel Parameters," in *Proc. IEEE 64th Vehicular Tech. Conf. (VTC-2006 Fall)*, Sep. 2006.

[54] K. Ravindra and A. Sarma, "Channel characterization of mobile signal at 11 GHz," in *Proc. Inter. Conf. on Electromagnetic Interference and Compatibility*, 2002.

[55] "Raplab (ray-tracing simulator)." [Online]. Available: http://www4.kke.co.jp/network/raplab/

[56] J. Fessler and A. Hero, "Space-alternating generalized expectation-maximization algorithm," *IEEE Trans. Signal Processing*, vol. 42, no. 10, pp. 2664–2677, Oct 1994.

[57] M. Bartlett, "Smoothing periodograms from time series with continuous spectra," *Nature*, vol. 161, 1948.

Publication List and Award

Journal

1. M. Kim, **Y. Konishi**, J. Takada and B. Gao, Automatic IQ Imbalance Compensation Technique for Quadrature Modulator by Single-Tone Testing, *IEICE Trans. Commun.*, Vol.E95-B,No.05, pp. 1864-1868, May 2012.

2. M. Kim, J. Takada, and **Y. Konishi**, A Novel Scalable MIMO Channel Sounding Technique and Measurement Accuracy Evaluation with Transceiver Impairments, *IEEE Trans. Instrum. Meas.*, vol. 61, no. 12, pp. 3185-3197, Dec. 2012.

3. **Y. Konishi**, M. Kim, Y. Chang and J. Takada, Versatile Radio Channel Sounder for Double Directional and Multi-link MIMO Channel Measurements at 11 GHz, *IEICE Trans. Electron.*, vol.E97-C, no.10, pp. 994-1004, Oct. 2014.

International Conference

1. J. Takada, **Y. Konishi**, B. Gao, M. Kim, S. Suyama, M. Ghoraishi and H. Suzuki, Development of 11 GHz MIMO Channel Sounder with 400 MHz Bandwidth using Software Radio Architecture, *EURO-COST2100,* Nov. 2010.

2. **Y. Konishi**, M. Kim, M. Gohraishi, J. Takada, S. Suyama and H. Suzuki, Channel Sounding Technique using MIMO Software Radio Architecture, in *Proc. European Conf. on Antennas and Propagation (EuCAP2010)*, Apr. 2011.

3. **Y. Konishi**, M. Kim and J. Takada, MIMO Channel Sounding Methodology for Future Mobile Communication Systems , in *Proc. 3rd Multidisciplinary Inter. Student Workshop (MISW2011)*, Jul. 2011.

4. J. Takada, **Y. Konishi**, B. Gao, M. Kim, S. Suyama, M. Ghoraishi and H. Suzuki, Development of 4×4 Full-MIMO Channel Sounder Operating at 11 GHz with 400 MHz Bandwidth Utilizing Software Radio Architecture, *URSI-General Assembly and Scientific Symposium*, Aug. 2011.

5. M. Kim, **Y. Konishi** and J. Takada, Effects of IQ Imbalance and Phase Noise in Fully Parallel MIMO Channel Sounder, *EURO-COST IC1004 4th Scientific Meeting*, Oct. 2011.

6. **Y. Konishi**, Y. Chang, M. Kim and J. Takada, Development of Versatile MIMO Channel Sounder for Double Directional and Multi-link Channel Characterizations at 11GHz, *EURO-COST IC1004 5th SM*, Sep. 2012.

7. M. Kim, **Y. Konishi**, Y. Chang and J. Takada, Measurement Results of Wideband Indoor MIMO Channel at 11 GHz, *EURO-COST IC1004 5th SM*, Sept. 2012.

8. Y. Chang, **Y. Konishi**, J. Shen, M. Kim and J. Takada, Indoor Wideband 8×12 MIMO Channel Analysis in an Exhibition Hall with Presence of People, *EURO-COST IC1004 5th SM*, Sept. 2012.

9. **Y. Konishi**, Y. Chang, M. Kim, Y. Maruichi, P. H. Van and J. Takada, Multi-link Indoor MIMO Measurements at 11 GHz using Scalable Wideband Channel Sounder, *2012 Inter. Symposium on Antennas and Propagation (ISAP2012)*, Oct. 2012.

10. Y. Chang, **Y. Konishi**, M. Kim and J. Takada, Calibration Techniques for Fully Parallel 24×24 MIMO Sounder, *2012 Inter. Symposium on Antennas and Propagation (ISAP2012)*, Oct. 2012.

Domestic Conference

1. **Y. Konishi**, M. Kim, S. Suyama, M. Ghoraishi, J. Takada and H. Suzuki, Development of Channel Sounder for Super High Bit-Rate Wireless Communication Systems, *IEICE Society Conf.*, Sep. 2010.

2. **Y. Konishi**, M. Kim, Mir Ghoraishi, J. Takada, S. Suyama and H. Suzuki, Channel Sounding Technique using MIMO Software Dened Radio Architecture, *IEICE TCSR*. Mar. 2011.

3. **Y. Konishi**, M. Kim, S. Suyama, M. Ghoraishi, J. Takada, H. Suzuki, 11GHz MIMO Channel Sounder using Software Radio Architecture, *IEICE General Conf.*, July 2011.

4. **Y. Konishi**, P. H. Van, Y. Maruichi, M. Kim, Mir Ghoraishi, and J. Takada, 11GHz MIMO Channel Sounder using Software Radio Architecture, *IEICE TCSR with Exhibition*. Jul. 2011.

5. Y. Maruichi, **Y. Konishi**, M. Kim and J. Takada, Wideband IQ Imbalance Compensation Technique for Quadrature Modulator, *IEICE-TCMW.*, Oct. 2011.

6. Y. Chang, **Y. Konishi**, M. Kim and J. Takada, Eigenvalues Analysis for Wideband 8×12 MIMO Indoor Measurement at 11GHz Frequency, *IEICE General Conf.*, Mar. 2012.

7. M. Kim, **Y. Konishi**, Y. Chang and J. Takada, Development of Wideband Scalable 24×24 MIMO Channel Sounder at 11 GHz, *IEICE-TCRSC*, May 2012.

8. **Y. Konishi**, Y. Chang, M. Kim, Y. Maruichi, P. H. Van and J. Takada, Indoor MIMO Multi-link Measurements at 11GHz,*IEICE-TCRCS*, Jul. 2012.

9. M. Kim, **Y. Konishi** and J. Takada, Highly Scalable Wideband MIMO Channel Sounding Technique, *IEICE Society Conf.*, Sep. 2012.

10. Y. Chang, **Y. Konishi**, J. Shen, M. Kim and J. Takada, Analysis for Wideband 8×12 MIMO Indoor Measurement at 11 GHz Frequency with Presence of People, *IEICE Society Conf.*, Sep. 2012.

Award

1. **Y. Konishi**, Best poster presentation award, *3rd Multidisciplinary Inter. Student Workshop*, 2011.

2. M. Kim, J. Takada, **Y. Konishi**, Telecommunications System Technology (TAF) Encourage Award, *29th TAF Telecommunications System Technology Encourage Award*, 2014.

Vita

Yohei Konishi received the B.E. degree in communication engineering from National Defense Academy, Japan, in 2005, and the M.E. degree in international development engineering from Tokyo Institute of Technology, Japan, in 2009. Since 2005, he has been a member of the Japan Grand Self Defense Force (JGSDF), Ministry of Defense, Japan.